Journal Pre-proof

STK11 Prevents Invasion Through STAT3/5 and FAK Repression in Cutaneous Melanoma.

Andreas Dzung, Annalisa Saltari, Natascia Tiso, Ruth Lyck, Reinhard Dummer, Mitchell P. Levesque

PII: S0022-202X(21)02466-0

DOI: https://doi.org/10.1016/j.jid.2021.09.035

Reference: JID 3192

To appear in: *The Journal of Investigative Dermatology*

Received Date: 20 November 2020

Revised Date: 23 August 2021

Accepted Date: 1 September 2021

Please cite this article as: Dzung A, Saltari A, Tiso N, Lyck R, Dummer R, Levesque MP, STK11 Prevents Invasion Through STAT3/5 and FAK Repression in Cutaneous Melanoma., *The Journal of Investigative Dermatology* (2021), doi: https://doi.org/10.1016/j.jid.2021.09.035.

STK11 Prevents Invasion Through STAT3/5 and FAK Repression in Cutaneous Melanoma.

Andreas Dzung[1*], Annalisa Saltari[1*], Natascia Tiso[2], Ruth Lyck[3],

Reinhard Dummer[1] & Mitchell P. Levesque[1]

[1]Department of Dermatology, University Hospital Zurich, University of Zurich, Zurich, Switzerland,

[2]Laboratory of Developmental Genetics, Department of Biology, University of Padova, Italy

[3]Theodor Kocher Institute, University of Bern, Bern, Switzerland

*these authors contributed equally to this work

Corresponding author:

Mitchell P. Levesque, University Hospital Zurich, University of Zurich, Wagistrasse 18, CH 8952 Schlieren, Switzerland

Tel: +41 44 556 32 62

e-mail: mitchell.levesque@usz.ch

Running title: Role of STK11 in melanoma

Keywords: Melanoma, metastasis, cancer biology, models zebrafish, signaling, STK11, LKB1, invasion

ABSTRACT

The serine/threonine kinase 11 (STK11/LKB1) is a tumor suppressor involved in metabolism and cell motility. In $BRAF^{V600E}$ melanoma, STK11 is inactivated by ERK and RSK, preventing it from binding and activating AMPK and promoting melanoma cell proliferation. Although STK11 mutations occur in 5-10% of cutaneous melanoma, few functional studies have been performed. By knocking out STK11 with CRISPR/Cas9 in two human BRAF-mutant melanoma cell lines, we found that STK11-loss reduced the sensitivity to a BRAF inhibitor (BRAFi). More strikingly, STK11 loss led to an increased invasive phenotype in both 3-dimensional spheroids and *in vivo* zebrafish xenograft models. STK11 overexpression consistently reverted the invasive phenotype.

Interestingly, STK11 knockout increased invasion also in an NRAS-mutant melanoma cell line. Furthermore, while STK11 was expressed in primary human melanoma tumors, its expression significantly decreased in melanoma metastases especially in brain metastases. In the STK11-knockout cells we observed increased activating phosphorylation of STAT3/5 and FAK. Using inhibitors of STAT3/5 and FAK, we reverted the invasive phenotype in both BRAF and NRAS mutated cells. Our findings confirm an increased invasive phenotype upon STK11-inactivation in BRAF and NRAS-mutant cutaneous melanoma that can be targeted by STAT3/5 and FAK-inhibition.

INTRODUCTION

The LKB1/*STK11* gene encodes a Serine/Threonine kinase, which is broadly expressed in all fetal and adult tissues although at different levels (Zhao and Xu, 2014). STK11 is known to directly phosphorylate and regulate adenosine monophosphate-activated protein kinase (AMPK) and 12 other AMPK-like kinases to regulate a broad spectrum of cellular functions including growth, metabolism, autophagy, adhesion, and polarity (Momcilovic and Shackelford, 2015). It was first reported to be a tumor suppressor when genetic loss of function alterations of STK11 were identified as the major cause of Peutz-Jeghers syndrome (PJS). PJS is a rare, autosomal dominant disease with hemizygotic loss of STK11 in 95-100% of the cases. It is characterized by the growth of gastrointestinal polyps, hyperpigmented freckling of the mouth and digits, and a strong predisposition for cancer in different organs, such as colon, pancreas, breast, ovary and testis. (Aretz et al., 2005; Daniell et al., 2018; Nagy et al., 2004) Moreover, STK11 mutations are frequently found in a variety of cancer patients without PJS, such as lung adenocarcinoma (30%), cervical carcinoma (15%) and melanoma (5-10%) (Forbes et al., 2011; Liu et al., 2012; Rowan et al., 1999). Due to its high mutation rate in lung cancer it has been frequently studied and was shown to increase lung cancer aggressiveness, metastasis, immune-evasion and recently, anti-PD1-inhibitor resistance (Koyama et al., 2016; Marcus and Zhou, 2010; Skoulidis et al., 2018).

In cutaneous melanoma, oncogenic $BRAF^{V600E}$, but not BRAF wildtype signaling, has been shown to functionally inhibit some STK11-dependent pathways (Zheng et al., 2009): Through increased ERK-activity from constitutive BRAF signaling, STK11 was unable to activate AMPK, a key metabolic enzyme, showing a linkage between the MAP-Kinase pathway with the STK11-AMPK pathway. These findings suggest an important role for the suppression of STK11 activity in $BRAF^{V600E}$-driven melanoma tumorigenesis (Zheng et al., 2009). Furthermore, the

inactivation of STK11 in a genetically engineered KRAS-mutant melanoma mouse model led to highly metastatic melanoma with 100% penetrance in a SRC-family kinase-dependent manner. As BRAF-mutant melanoma represents around 50% of cutaneous melanomas (Schadendorf et al., 2018), we sought to study the effects of genetic STK11-inactivation in $BRAF^{V600E}$-mutant human melanoma cells on BRAF-inhibitor resistance and invasion. We then confirmed our findings in an NRAS melanoma cell line.

RESULTS

STK11-Loss Reduces Sensitivity to BRAF^{V600E}-Inhibitor.

To explore the role of STK11-inactivation in melanoma we created stable STK11-knockouts (STK11-KO) using the Clustered Regularly Interspaced Short Palindromic Repeats (CRISPR) and CRISPR-associated protein-9 nuclease CRISPR/Cas9 system (Jinek et al., 2012) with three different short-guide RNAs, each targeting a different exon in the STK11-transcript (Figure 1A). To rule out differences based on cell line heterogeneity, we generated monoclonal cell lines from 2 BRAF^{V600E} (M990922 and WM793B) and 1 NRAS^{Q61R} (M130425) mutated melanoma cell cultures. For each cell line we expanded single cell clones with a successful knock-out of at least two different exons and one single cell clone harboring a non-targeting scramble (SCR) short-guide RNA construct with wildtype STK11 (Figure 1B and Supplementary Figure S1A). Although STK11-KO2 in both BRAF mutated cell lines showed a significant increase in cell growth at 3 days in comparison to controls, the same effect was not observed in NRAS mutated cells (Supplementary Figure S1B-S1C). Altogether, we observed no difference in the proliferation rate between the STK11-KO cells and the SCR cells (Supplementary Figure S1D).

We then investigated, whether STK11 loss-of-function affected the sensitivity to the BRAF-inhibitor (LGX) and the MEK inhibitor (MEK162). In a 2-dimensional (2D) assay, STK11 loss resulted in a significantly decreased susceptibility to LGX compared to the SCR at both 3 and 6 days, suggesting a role for STK11 in drug resistance (Figure 1C). In contrast, no reduction in the sensitivity towards MEK162 was observed in the NRAS^{Q61R}-mutated cell line M130425 after STK11-silencing (Figure 1C). A similar result was shown at 14 days, in a long-term colony formation assay (Figure 1D). To confirm the reduced sensitivity to LGX observed in 2D, we

generated 3dimensional (3D) spheroids from M990922 and WM793B cell lines (Supplementary Figure S1E).

We then treated the 3D-spheroids with LGX and performed a live (green)/ dead (red) staining observing a significantly higher number of dead cells in the SCR spheres compared to the STK11-KO cells (Figure 1E).

To evaluate the role of STK11 in acquired drug resistance, we measured STK11 levels in five BRAFi-sensitive (S) cells before and after rendering them BRAFi-resistant (R) in vitro (Supplementary Figure S2A). As expected, STK11 was reduced in M990922-R and WM793B-R compared to their sensitive counterparts M990922-S and WM793B-S (Supplementary Figure S2B). The same result was observed in SKMEL28-R compared to SKMEL-S cells. However, a reduction of STK11 after LGX acquired resistance was observed in 3 out of 5 paired cell lines revealing that STK11 plays a role in drug resistance in a subset of BRAF-muted melanoma cells. Together, these data suggest that a subtype of melanoma cells profits from a STK11-loss of function under MAPK-inhibition.

STK11 Knockout Prevents Activation of the AMPK-RAPTOR Pathway Upon BRAFi Treatment.

Hyperactive MAPK-signaling in $BRAF^{V600E}$-mutant melanoma suppresses the interaction between STK11 and AMPK through strong phospho-ERK1/2 signaling (Zheng et al., 2009). We therefore hypothesized that in STK11 expressing $BRAF^{V600}$-mutant melanoma, the tumor suppressive STK11-AMPK axis is inhibited through $BRAF^{V600E}$-signaling (Figure 2A, left). We hypothesized that under BRAF-inhibition, STK11 could restore its tumor suppressive function and induce Raptor signaling through AMPK activation (Figure 2A, middle). Finally, in STK11-

KO cells, we expect that the activation of the AMPK-Raptor pathway upon BRAF-inhibition is prevented and associated with increased resistance (Figure 2A, right).

To test this hypothesis, we treated the transgenic M990922 and WM793 constructs with LGX for up to 72 hours. LGX-treatment effectively reduced the phosphorylation of the $BRAF^{V600E}$ downstream kinase ERK1/2 (Figure 2B). Interestingly, in the SCR clones, STK11-levels increased upon LGX treatment confirming the role of $BRAF^{V600E}$ in inhibiting STK11 activity (Figure 2B). As expected, AMPKα1 threonine 172-phosphorylation increased under LGX treatment, indicating increased AMPKα1 activation (Figure 2B). In contrast, AMPKα1-activation was prevented in STK11-KO cells. Consistently, phosphorylation of the AMPKα1-target Raptor serine 172, was induced in the SCR cells under treatment but not in STK11-KO cells (Figure 2B).

To evaluate whether the inhibition of the AMPKα1-Raptor axis in STK11-KO clones could be reverted, we treated WM793B and M990922 STK11-KO cells with AICAR, an analog of adenosine monophosphate (AMP) capable of stimulating AMPK activity (Figure 2C). Interestingly, AMPK phosphorylation was restored in the presence of AICAR and resulted in a significant decrease in melanoma viability in STK11-KO clones (Figure 2C-2D). Moreover, the administration of AICAR increased the effectiveness of the BRAFi by significantly reducing cell viability in comparison to the single treatment (Figure 2E).

STK11 Loss Induces Invasion of $BRAF^{V600E}$ and $NRAS^{Q61R}$ Melanoma Cells *in vitro.*

As the loss of STK11 has been recently shown to increase metastasis in a genetically modified mouse KRAS-mutant model (Liu et al., 2012), we assessed the effect of STK11-loss on invasion in BRAF-mutated melanoma. First, we tested the ability of the STK11 clones to adhere to dermal

microvascular (HMEC1) and blood-brain barrier (HDMEC/D3) endothelial cells. The adhesion of STK11-KO cells to the monolayer of endothelial cells, was significantly higher compared to SCR cells, suggesting a greater ability to invade the tumor microenvironment (Figure 3A).

To measure the invasive abilities of STK11-KO cells, we embedded 3D-multicellular spheroids of the BRAF mutated transgenic cell lines into collagen I. Over 7 and 16 days, the STK11-KO cells displayed a significantly increased invasion, as compared to the SCR cells (Figure 3B). Interestingly, a similar result was observed after STK11-KO in the $NRAS^{Q61R}$ M130425 cells, which displayed a significantly higher invasive phenotype compared to the M130425 SCR cells (Figure 3C). Notably, the treatment of spheres derived from BRAF-mutated cells with LGX, led to a strong reduction of collagen invasion in all the transgenic constructs (Supplementary Figure S3A-S3B). However, while invasion was completely prevented by LGX in the SCR cell lines, the STK11-KO cells showed minimal residual invasive capabilities under BRAF-inhibition displaying a higher invasion area compared to the SCR cells. Moreover, while spheres derived from SCR cells were dead after treatment with LGX, as shown by the live/dead staining (Supplementary Figure S3C), those derived from STK11-KO cells, not only displayed a residual invasive capacity, but they were also alive, thus confirming a reduced sensitivity to BRAFi-treatment. Strikingly, STK11-overexpression in M150536, a $BRAF^{V600E}$-mutant melanoma derived from brain metastasis, with low endogenous STK11-expression and a highly invasive phenotype, led to abrogation of invasion without affecting viability, while the spheres derived from the empty vector (EV) control cells strongly invaded into the collagen I matrix (Figure 3D and Supplementary Figure S4A-B). We therefore conclude that STK11 has an inhibitory function on invasion in human cutaneous melanoma cells.

STK11 Loss Is Associated with Increased Metastasis in Zebrafish Xenografts and in Human Melanoma Tumors.

To evaluate the effects of STK11-KO *in vivo*, we injected M990922 and WM793B STK11-constructs into the yolk of 2-day old zebrafish larvae, exposed them to LGX 1 day post-injection (dpi) and assessed the survival and metastasis formation at 6dpi. At 1dpi, melanoma cells were confined to the yolk of zebrafish larvae (Supplementary Figure S5A). However, at 6dpi, STK11-KO cells strongly migrated from the yolk to other tissues showing a significantly higher number of zebrafish with metastasis in comparison to SCR cells (Figure 4A-4B). No difference in survival was observed between the xenografts, except for a higher mortality of M990922 STK11-KO injected zebrafish (Supplementary Figure S5B). Consistent with the *in vitro* results in the presence of LGX, STK11-KO injected larvae displayed residual invading cells as shown by the significantly higher percentage of metastases (Figure 4A-4B and Supplementary Figure S5C). Interestingly, the analysis of the sites of metastasis revealed an increased occurrence of brain metastases in WM793B STK11-KO cells (Supplementary Figure S5D).

As loss of function mutations of STK11 are less common in melanoma (10%) (Forbes et al., 2011; Rowan et al., 1999), we wondered whether the expression of STK11 changes during the course of melanoma progression. We thus evaluated STK11 and S100-expression, a marker for melanoma cells (Jungbluth and Busam, 2019) in three tissue micro arrays (TMAs) derived from primary melanoma tumors (n=166), melanoma metastases from different non-cranial organ sites (n=82), and melanoma brain metastases (N=70) (Figure 4C). In primary melanoma tumors, STK11 was high and heterogeneously expressed. Moreover, STK11 levels were significantly lower in melanoma metastases in comparison to primary melanomas, with the lowest expression in brain metastases (Figure 4C and 4D).

STK11 Loss Enhanced Activation of STAT3/5 and FAK.

To identify the pathways involved in STK11-inactivation induced invasion and metastasis, we performed a phospho-kinase protein array in M990922 cells (Figure 5A). We observed a significantly higher activation of STAT3, STAT5a/b, and FAK in STK11-KO in comparison to SCR cells (Figure 5B). Moreover, the phosphorylation of these proteins was stronger in both BRAF and NRAS mutated STK11-KO cells (Figure 5C). Consistently, STK11 overexpression in M150536 cells strongly reduced phosphorylation of STAT3, STAT5a/b, and FAK (Supplementary Figure S6A). Furthermore, upon LGX administration p-ERK was reduced both in SCR and STK11-KO cells, while AMPK phosphorylation was detected only in SCR but not in STK11-KO cells, confirming the role of STK11 in AMPK activation. Finally, pSTAT5a/b was significantly higher in STK11-KO cells irrespective of the presence of the BRAFi (Figure 5D).

STK11 Loss-Mediated Invasion Is Prevented by STAT3/5- and FAK-inhibition.

We next tested the effect of STAT3/5 (C188-9 and SH-4-54) and FAK (PF-573228) inhibitors on viability and invasion of 3D-spheroids under increasing drug concentrations (Supplementary Figure S6B). Interestingly, the inhibition of STAT3/5 or FAK strongly reduced the invasive abilities of M990922 and WM793B STK11-KO cells without affecting melanoma viability. Quantification of the spheroid area revealed a significantly reduced invasion of STK11-KO spheres after treatment with two different STAT3/5i or a FAKi in both M990922 and WM793B cells (Figure 6B-D). A similar result was observed after administration of both drugs in combination, with an induction of cell death in the presence of the highest concentrations (Supplementary Figure S6C-S6D). Noteworthy, a similar result could be observed in the

NRASQ61R-mutant M130425 STK11-KO cells, especially after FAK inhibition (Figure 6D and S7A-B). We therefore conclude that STK11 loss is associated with an increased invasive phenotype *in vitro* and *in vivo*, which can be reverted by the inhibition of STAT3/5 and FAK in both BRAF and NRAS -mutated melanoma cells (Figure 6E).

DISCUSSION

The role of the tumor suppressor STK11 has been frequently studied in many cancers, often in the context of invasion and metastasis (Marcus and Zhou, 2010; Momcilovic and Shackelford, 2015; Zhao and Xu, 2014). Loss of STK11 has also been associated with immune evasion and decreased response in immune-checkpoint inhibitor therapy in lung cancer (Koyama et al., 2016; Skoulidis et al., 2018). However, its role in melanoma remains to be extensively investigated. This study highlights the role of STK11 in melanoma drug response, and invasion. The evaluation of drug response revealed a reduced sensitivity in two STK11-KO cell lines towards BRAF-inhibition, both *in vitro* and *in vivo*. The higher sensitivity of STK11 SCR cells to BRAFi, was associated with the activation of the STK11-AMPK-RAPTOR pathway, suggesting mTOR inactivation, a known marker of melanoma survival and resistance (Kozar et al., 2019; Rossi et al., 2019). However, these results were only observable in some cell lines, suggesting that a resistance-promoting effect of STK11-loss may only be true in a subset of melanoma, which needs to be further elucidated.

We observed that the most dramatic difference in STK11-KO cells was increased invasiveness. Compared to the SCR cells, the STK11-KO cells displayed an enhanced adhesion to endothelial cells, and a strong invasion in a 3D-multicellular spheroid model. The same finding was observed also in $NRAS^{Q61R}$-mutant melanoma cells. Consistently, STK11-KO cells were more invasive in an *in vivo* zebrafish xenograft model, showing a significantly higher percentage of metastases in comparison to SCR injected larvae. In contrast, STK11 overexpression reverted the strong invasive phenotype in melanoma spheroids with low STK11 expression. These observations strengthen previous findings in KRAS-mutant melanoma mouse models (Liu et al.,

2012) and reveal that STK11-inactivation increases invasion also in a $BRAF^{V600E}$ and $NRAS^{Q61R}$-mutant background.

While STK11 loss of function mutations are less frequent in melanoma than in other cancers (10% and less) (Forbes et al., 2011), non-genetic mechanisms of STK11 inactivation can take place, such as epigenetic inactivation, decreased expression or biological inactivation (Zhou et al., 2014). The evaluation of STK11 expression on melanoma TMAs revealed that STK11 was highly expressed in primary tumors but significantly decreased in metastases, with the lowest levels observed in brain metastases. This finding is consistent with previous observations in non-small-cell lung carcinoma where an oncogenic KRAS mutation and low STK11 copy number was shown to be associated with brain metastasis (Zhao et al., 2014). Additionally, STK11 deletion is frequently shown in brain metastases of different carcinomas (Sobottka et al., 2000).

To investigate the mechanisms driving the enhanced invasion in STK11-KO cells, we performed a phospho-kinase array. In the STK11-KO cells we identified increased activating phosphorylation of STAT3 (serine727 and tyrosine705), STAT5A/B (tyrosine694/699) and FAK (tyrosine397).

Increased activity of p-STAT3 upon STK11 loss or downregulation has been shown in many cancers: In papillary thyroid carcinoma cells STK11 was shown to inhibit STAT3-activation via RET/PTC-inhibition (Kim et al., 2007). In addition, STK11 directly interacted with STAT3, leading to the suppression of STAT3-mediated gene expression. In contrast, STK11-knockdown resulted in increased activation of STAT3 and cell proliferation. In gastrointestinal cancer, loss of STK11 in stromal fibroblasts was associated with the induction of the IL-11/JAK/STAT3 pathway, which resulted in fully penetrant polyposis in mice (Ollila et al., 2018). Interestingly, in a PJS-mouse model, the heterozygous deletion of STK11 in T cells was sufficient to promote

gastrointestinal polyp formation, STAT3 activation, and increased IL-6, IL-11 and CXCL2 expression (Poffenberger et al., 2018). Moreover, STAT3 has been consistently associated with migration, invasion, and metastasis in many cancers including melanoma, where STAT3 activation promoted melanoma brain metastasis in a xenograft mouse model (Kulesza et al., 2019; Teng et al., 2014; Xie et al., 2006).

While the regulation of STAT5A/B through STK11 has not been extensively studied, it has been frequently associated with metastasis in different cancers. In prostate cancer p-STAT5 Y694/699 promoted metastatic behavior and JAK2-STAT5A/B signaling was critical for the induction of epithelial-mesenchymal transition (Gu et al., 2010; Talati et al., 2015). In colorectal cancer, STAT5 silencing induced cell cycle arrest and reduced tumor cell invasion (Xiong et al., 2009). In melanoma, more malignant and metastatic phenotypes were governed by the scavenger receptor SR-BI which in turn activated STAT5 through glycosylation (Kinslechner et al., 2018).

Finally, the focal adhesion kinase FAK/PTK2 is another well described target of STK11, which has been studied in adhesion, invasion, and metastatic processes. In lung cancer cells, STK11 forms a complex with FAK to repress its activation, thereby inhibiting the adhesion to fibronectin (Kline et al., 2013). Likewise, in a lung cancer mouse model with KRAS hyperactivation and STK11 loss, a strong FAK activation occurred in collectively invasive cells. When these cells were tested in a 3D invasion model, the loss of STK11, but not P53, was sufficient to drive invasion, which was highly sensitive to FAK inhibition (Gilbert-Ross et al., 2017). In aggressive uveal and cutaneous melanoma cells, FAK was phosphorylated on its key tyrosine residues (Y397 and Y576) and correlated with increased invasion and migration (Hess et al., 2005).

The inhibition of STAT3/5 and FAK in STK11-KO melanoma cells had no effect on 3D spheroid viability, but successfully reverted their invasive phenotype. These results highlight the prognostic role of STK11-loss in melanoma metastasis and could help for a stratification in which STAT3/5 and/or FAK-inhibition are beneficial in the management of STK11-loss-mutated metastatic cutaneous melanoma.

MATERIAL AND METHODS

Cell Culture

Human melanoma cells were obtained from the University Research Priority Program (URPP) melanoma biobank Zurich according to ethics approval BASEC-Nr.2017-00494 after written, informed consent or from the American Type Culture Collection (ATCC) and cultured as described in Supplementary Material. Ethical approval to conduct the experiments described here was provided by the Kantonal Ethics Commission Zurich: KEK-ZH-Nr.2014-0425.

Transgenic cell lines

Transgenic knock-out cell lines of STK11 were generated with the CRISPR/Cas9 system as indicated in Supplementary Material. For transduction of melanoma cells, the virus-containing medium was added together with PEImax and polybrene (8µg/mL). GFP-positive cells were sorted as single cells by the FACSAria™ III fluorescence-activated cell sorter (BD Biosciences).

Colorimetric Resazurin-based viability assay:

Cells were seeded into 96-well plates and treated 1d post-seeding with LGX818 (Selleckchem, Cat.no. S7108), AICAR (Selleckchem, Cat.No. S1802) and viability was assessed as indicated in Supplementary Material.

Colony formation assay:

100 or 500 cells/well were seeded in 12-well plates and treated with LGX. Medium was changed every 72h. The staining and the quantification of the number of colonies was perfomed as indicated in Supplementary Material.

3D-multicellular spheroid assay and spheroid collagen invasion assay:

3D-melanoma spheroids were obtained by seeding melanoma cells on previously coated agarose plate. The spheroids were treated for drug response assessment or embedded into a collagen I-mixture as indicated in Supplementary Material. The spheres viability was assessed by calcein AM (live) (Sigma, Cat.No. 17783) and ethidium homodimer (death) stain (Sigma, Cat.No. 46043) as indicated in Supplementary Material.

Endothelial-melanoma cell-cell adhesion assay:

The imicrovascular endothelial cells hMEC1 and hCMEC/D3 were seeded into a 4-well chamber slide (Falcon, Cat.No. 354114) (25’000 cells per 1.7cm^2 chamber) and grown to 100% confluency (ca 4d). Melanoma cells were stained with Vybrant DiI (1 µg/mL, ThermoFisher, Cat.No. V22885) and incubated at 37°C with endothelial monolayers. The evaluation of adherent cells was performed as indicated in Supplementary Material.

Western Blots:

Protein extracts were obtained by using the cell lysis buffer (NaCl 150mM, MgCl2 15mM, EGTA 1mM, Hepes 50mM, Glycerol 10%, Triton-X 1%) and Western Blot was performed as indicated in Supplementary Material. Antibodies used: STK11 (CST #3047), ERK1/2 (CST #4695), p-ERK1/2 T202/Y204 (CST# 4376), STAT3 (CST #9132), p-STAT3 Y705 (#9138), p-STAT3 S727 (CST #9134), FAK (CST #3285), p-FAK Y397 (CST #3283), p-STAT5A/B Y699/Y694 (CST #9359S).

Immunohistochemistry:

The TMAs of primary melanomas were a gift from the URPP biobank Zurich, University Hospital Zurich, Switzerland (Mitch Levesque), while the TMA from non-cranial melanoma metastases was purchased from Biomax (Cat.No. BCC38218). The TMA from brain metastasis was described before[51]. Immunohistochemistry was performed on tissue microarrays (TMAs) by using as indicated in Supplementary Material.

Human Phospho-Kinase Array Kit

The Proteome Profiler Human Phospho-Kinase Array Kit (R&D systems, Cat. No. ARY003B) was performed as indicated by the manufacturer. The quantification of phosphorylated protein was performed as indicated in Supplementary Material.

Zebrafish husbandry

Fish maintenance and handling was carried out in accordance with European and Italian law on animal experimentation (D.L. 4 March 2014, no. 26), under authorization no. 407/2015-PR from the Italian Ministry of Health (Vito et al., 2020). Zebrafish experiments were performed in collaboration with Professor Natascia Tiso at the zebrafish facility of the University of Padova, Italy. Larvae were injected at 2 days after fertilization with melanoma cells as indicated in the Supplementary Materials.

Statistical analysis

All statistical analysis were performed using GraphPad Prism 5.0. P values ≤ 0.05 were considered significant. All experiments were performed in triplicates and error bars represent the mean ± S.D.

DATA AVAILABILITY STATEMENT

The authors declare that the data supporting the findings of this study are available within the paper and its supplementary information files are available from the authors upon request. No datasets were generated or analyzed during the current study.

ORCIDS

Andreas Dzung: https://orcid.org/0000-0002-1776-1928

Annalista Saltari: https://orcid.org/0000-0002-8621-4039

Natascia Tiso: https://orcid.org/0000-0002-5444-9853

Ruth Lyck: https://orcid.org/0000-0002-6479-4837

Reinhard Dummer: https://orcid.org/0000-0002-2279-6906

Mitchell Paul Levesque: https://orcid.org/0000-0001-5902-9420

CREDIT STATEMENT (AUTHOR CONTRIBUTIONS)

Conceptualization: AD, AS, MPL; Data curation: AD, AS; Formal analysis: AD, AS; Funding acquisition: ML; Investigation: AD, AS, NT; Resources: NT, RL, MPL; Visualization: AD, AS, NT; Writing: AD, AS, NT, RL, MPL

ACKNOWLEDGMENTS

We thank Florian Olomski for his expertise in cloning. We thank Phil Cheng and Patrick Turko for biostatistical analyses. We further thank Federica Sella (University Hospital Zurich) for the immunohistochemical stains, Melanie Maudrich, Jan Kaesler, and Corinne Stoffel for help in various experiments in the laboratory (University Hospital Zurich).

CONFLICT OF INTEREST

The authors state no conflicts of interest concerning this work. Prof. Dummer has intermittent, project focused consulting and/or advisory relationships with Novartis, Merck Sharp & Dhome (MSD), Bristol-Myers Squibb (BMS), Roche, Amgen, Takeda, Pierre Fabre, Sun Pharma, Sanofi, Catalym, Second Genome, Regeneron, Alligator, MaxiVAX SA and touchIME outside the submitted work. Prof. Levesque receives project-related funding outside the scope of this work from Roche, Novartis, Molecular Partners, and Oncobit AG.

REFERENCES

Aretz S, Stienen D, Uhlhaas S, Loff S, Back W, Pagenstecher C, et al. High proportion of large genomic STK11 deletions in Peutz-Jeghers syndrome. Hum Mutat 2005;26:513–9. https://doi.org/10.1002/humu.20253.

Daniell J, Plazzer J-P, Perera A, Macrae F. An exploration of genotype-phenotype link between Peutz-Jeghers syndrome and STK11: a review. Fam Cancer 2018;17:421–7. https://doi.org/10.1007/s10689-017-0037-3.

Forbes SA, Bindal N, Bamford S, Cole C, Kok CY, Beare D, et al. COSMIC: mining complete cancer genomes in the Catalogue of Somatic Mutations in Cancer. Nucleic Acids Res 2011;39:D945-950. https://doi.org/10.1093/nar/gkq929.

Gilbert-Ross M, Konen J, Koo J, Shupe J, Robinson BS, Wiles WG, et al. Targeting adhesion signaling in KRAS, LKB1 mutant lung adenocarcinoma. JCI Insight 2017;2:e90487. https://doi.org/10.1172/jci.insight.90487.

Gu L, Vogiatzi P, Puhr M, Dagvadorj A, Lutz J, Ryder A, et al. Stat5 promotes metastatic behavior of human prostate cancer cells in vitro and in vivo. Endocr Relat Cancer 2010;17:481–93. https://doi.org/10.1677/ERC-09-0328.

Hess AR, Postovit L-M, Margaryan NV, Seftor EA, Schneider GB, Seftor REB, et al. Focal Adhesion Kinase Promotes the Aggressive Melanoma Phenotype. Cancer Res 2005;65:9851–60. https://doi.org/10.1158/0008-5472.CAN-05-2172.

Jinek M, Chylinski K, Fonfara I, Hauer M, Doudna JA, Charpentier E. A programmable dual-RNA-guided DNA endonuclease in adaptive bacterial immunity. Science 2012;337:816–21. https://doi.org/10.1126/science.1225829.

Jungbluth AA, Busam KJ. 29 - Immunohistochemistry for the Diagnosis of Melanocytic Proliferations. In: Busam KJ, Gerami P, Scolyer RA, editors. Pathol. Melanocytic Tumors, Philadelphia: Elsevier; 2019, p. 348–63. https://doi.org/10.1016/B978-0-323-37457-6.00029-8.

Kim DW, Chung HK, Park KC, Hwang JH, Jo YS, Chung J, et al. Tumor Suppressor LKB1 Inhibits Activation of Signal Transducer and Activator of Transcription 3 (STAT3) by Thyroid Oncogenic Tyrosine Kinase Rearranged in Transformation (RET)/Papillary Thyroid Carcinoma (PTC). Mol Endocrinol 2007;21:3039–49. https://doi.org/10.1210/me.2007-0269.

Kinslechner K, Schörghofer D, Schütz B, Vallianou M, Wingelhofer B, Mikulits W, et al. Malignant Phenotypes in Metastatic Melanoma are Governed by SR-BI and its Association with Glycosylation and STAT5 Activation. Mol Cancer Res MCR 2018;16:135–46. https://doi.org/10.1158/1541-7786.MCR-17-0292.

Kline ER, Shupe J, Gilbert-Ross M, Zhou W, Marcus AI. LKB1 Represses Focal Adhesion Kinase (FAK) Signaling via a FAK-LKB1 Complex to Regulate FAK Site Maturation and Directional Persistence. J Biol Chem 2013;288:17663–74. https://doi.org/10.1074/jbc.M112.444620.

Koyama S, Akbay EA, Li YY, Aref AR, Skoulidis F, Herter-Sprie GS, et al. STK11/LKB1 Deficiency Promotes Neutrophil Recruitment and Proinflammatory Cytokine Production to Suppress T-cell Activity in the Lung Tumor Microenvironment. Cancer Res 2016;76:999–1008. https://doi.org/10.1158/0008-5472.CAN-15-1439.

Kozar I, Margue C, Rothengatter S, Haan C, Kreis S. Many ways to resistance: How melanoma cells evade targeted therapies. Biochim Biophys Acta BBA - Rev Cancer 2019;1871:313–22. https://doi.org/10.1016/j.bbcan.2019.02.002.

Kulesza DW, Przanowski P, Kaminska B. Knockdown of STAT3 targets a subpopulation of invasive melanoma stem-like cells. Cell Biol Int 2019;43:613–22. https://doi.org/10.1002/cbin.11134.

Liu W, Monahan KB, Pfefferle AD, Shimamura T, Sorrentino J, Chan KT, et al. LKB1/STK11 Inactivation Leads to Expansion of a Prometastatic Tumor Subpopulation in Melanoma. Cancer Cell 2012;21:751–64. https://doi.org/10.1016/j.ccr.2012.03.048.

Marcus AI, Zhou W. LKB1 regulated pathways in lung cancer invasion and metastasis. J Thorac Oncol Off Publ Int Assoc Study Lung Cancer 2010;5:1883–6. https://doi.org/10.1097/JTO.0b013e3181fbc28a.

Momcilovic M, Shackelford DB. Targeting LKB1 in cancer – exposing and exploiting vulnerabilities. Br J Cancer 2015;113:574–84. https://doi.org/10.1038/bjc.2015.261.

Nagy R, Sweet K, Eng C. Highly penetrant hereditary cancer syndromes. Oncogene 2004;23:6445–70. https://doi.org/10.1038/sj.onc.1207714.

Ollila S, Domènech-Moreno E, Laajanen K, Wong IPL, Tripathi S, Pentinmikko N, et al. Stromal Lkb1 deficiency leads to gastrointestinal tumorigenesis involving the IL-11–JAK/STAT3 pathway. J Clin Invest 2018;128:402–14. https://doi.org/10.1172/JCI93597.

Poffenberger MC, Metcalfe-Roach A, Aguilar E, Chen J, Hsu BE, Wong AH, et al. LKB1 deficiency in T cells promotes the development of gastrointestinal polyposis. Science 2018;361:406–11. https://doi.org/10.1126/science.aan3975.

Rossi A, Roberto M, Panebianco M, Botticelli A, Mazzuca F, Marchetti P. Drug resistance of BRAF-mutant melanoma: Review of up-to-date mechanisms of action and promising targeted agents. Eur J Pharmacol 2019;862:172621. https://doi.org/10.1016/j.ejphar.2019.172621.

Rowan A, Bataille V, MacKie R, Healy E, Bicknell D, Bodmer W, et al. Somatic mutations in the Peutz-Jeghers (LKB1/STKII) gene in sporadic malignant melanomas. J Invest Dermatol 1999;112:509–11. https://doi.org/10.1046/j.1523-1747.1999.00551.x.

Schadendorf D, van Akkooi ACJ, Berking C, Griewank KG, Gutzmer R, Hauschild A, et al. Melanoma. The Lancet 2018;392:971–84. https://doi.org/10.1016/S0140-6736(18)31559-9.

Skoulidis F, Goldberg ME, Greenawalt DM, Hellmann MD, Awad MM, Gainor JF, et al. STK11/LKB1 Mutations and PD-1 Inhibitor Resistance in KRAS-Mutant Lung Adenocarcinoma. Cancer Discov 2018;8:822–35. https://doi.org/10.1158/2159-8290.CD-18-0099.

Sobottka SB, Haase M, Fitze G, Hahn M, Schackert HK, Schackert G. Frequent Loss of Heterozygosity at the 19p13.3 Locus Without LKB1/STK11 Mutations in Human Carcinoma Metastases to the Brain. J Neurooncol 2000;49:187–95. https://doi.org/10.1023/A:1006442024874.

Talati PG, Gu L, Ellsworth EM, Girondo MA, Trerotola M, Hoang DT, et al. Jak2-Stat5a/b Signaling Induces Epithelial-to-Mesenchymal Transition and Stem-Like Cell Properties in Prostate Cancer. Am J Pathol 2015;185:2505–22. https://doi.org/10.1016/j.ajpath.2015.04.026.

Teng Y, Ross JL, Cowell JK. The involvement of JAK-STAT3 in cell motility, invasion, and metastasis. JAK-STAT 2014;3. https://doi.org/10.4161/jkst.28086.

Xie T, Huang F-J, Aldape KD, Kang S-H, Liu M, Gershenwald JE, et al. Activation of Stat3 in Human Melanoma Promotes Brain Metastasis. Cancer Res 2006;66:3188–96. https://doi.org/10.1158/0008-5472.CAN-05-2674.

Xiong H, Su W-Y, Liang Q-C, Zhang Z-G, Chen H-M, Du W, et al. Inhibition of STAT5 induces G1 cell cycle arrest and reduces tumor cell invasion in human colorectal cancer cells. Lab Invest 2009;89:717–25. https://doi.org/10.1038/labinvest.2009.11.

Zhao N, Wilkerson MD, Shah U, Yin X, Wang A, Hayward MC, et al. Alterations of LKB1 and KRAS and Risk of Brain Metastasis: Comprehensive Characterization by Mutation Analysis, Copy Number, and Gene Expression in Non-Small-Cell Lung Carcinoma. Lung Cancer Amst Neth 2014;86:255–61. https://doi.org/10.1016/j.lungcan.2014.08.013.

Zhao R-X, Xu Z-X. Targeting the LKB1 Tumor Suppressor. Curr Drug Targets 2014;15:32–52.

Zheng B, Jeong JH, Asara JM, Yuan Y-Y, Granter SR, Chin L, et al. Oncogenic B-RAF Negatively Regulates the Tumor Suppressor LKB1 to Promote Melanoma Cell Proliferation. Mol Cell 2009;33:237–47. https://doi.org/10.1016/j.molcel.2008.12.026.

Zhou W, Zhang J, Marcus AI. LKB1 tumor suppressor: Therapeutic opportunities knock when LKB1 is inactivated. Genes Dis 2014;1:64–74. https://doi.org/10.1016/j.gendis.2014.06.002.

FIGURE LEGENDS

Figure 1. STK11 Loss reduces sensitivity to BRAF^{V600E}-Inhibitor.

a) STK11-KO sgRNA (KO 1-3) targets on different exon on the STK11 transcript. b) Western Blot of SCR and STK11-KO clones. c) STK11 SCR and STK11-KO clones were seeded in 96-well plates. 1 day later, cells were treated with LGX 10nM or MEK162 10nM and viability was measured by Resazurin assay 3d and 6d later. d) Colony formation assay. 3500 cells/well were seeded into a 24-well plate and treated with LGX 10nM. E) 4000 cells per well were seeded in agar-coated plates until spheres formed and treated with LGX 50nM for 3d and 6d. Live/dead ratios were assessed by Calcein-AM/Ethidium-homodimer staining. Scale bar = 1000µm. Data represent the mean ± S.D. of triplicate determinations. Two-way Anova was used for statistical analysis *p<0.05; **p<0.01; ***p<0.001; ****p<0.00001

Figure 2. Activation of AMPK-RAPTOR Pathway Upon BRAFi is Prevented in STK11 Knockout Cells.

a) Model explaining the loss of the tumor suppressive function of the STK11-AMPKα axis in STK11-KO cells. b) WB of M990922 and WM793B under treatment with LGX 20nM. c) Western Blot of M990922 and WM793B with the AMPK-activator AICAR (1mM) alone or in combination with LGX (20nM). d and e) 2D viability assay under 6d of AICAR mono-treatment or in combination with LGX by Resazurin. Data represent the mean ± S.D. of triplicate

determinations. Two-way Anova was used for statistical analysis *p<0.05; **p<0.01; ***p<0.001; ****p<0.00001

Figure 3. STK11 Loss Induces Invasion of BRAF^{V600E} and NRAS^{Q61R} Melanoma Cells *in vitro*

a) Cellular adhesion assay. Human microvascular endothelial cells hMEC1 (skin-derived) and hCMEC/D3 (blood-brain barrier derived) were seeded and grown to 100% confluency. Melanoma cells were starved for 24h, fluorescently labeled and 25'000 cells were seeded per cell culture chamber. After an incubation of 30min at 37°C the chambers were washed and the number of adhered and fluorescently labeled cells was assessed. Scale bar = 100µm. b-c) 3D multicellular spheroid invasion into collagen. After spheroid formation, the spheres were embedded into collagen and assessed for invasion at 7 and 16 days (BRAF mut) and 9 days (NRAS mut). Scale bar = 500µm. Data represent the mean ± S.D. of triplicate determinations. Two-way Anova was used for statistical analysis *p<0.05; **p<0.01; ***p<0.001 d) Calcein AM/Ethidium homodimer staining was used to evaluate the spheres viability. n = 15 spheres/condition. Scale bar = 500µm. Data represent the mean ± S.D. of triplicate determinations. Two-way Anova was used for statistical analysis *p<0.05; **p<0.01; ***p<0.001; ****p<0.00001

Figure 4. STK11 Loss Is Associated with Increased Metastasis in Zebrafish Xenografts and in Melanoma Patients

a) M990922 and WM793B cells were injected into the yolk of 2 days post-fertilization (dpf) old zebrafish as a single droplet (100 µm diameter, about 100 cells/embryo). Scale bar = 500µm. b) The numbers of zebrafish with metastases was assessed at 6 dpf by a blind investigator. Data represents the mean ± S.D. of triplicate determinations. Two-way Anova was used for statistical analysis *p<0.05; **p<0.01; ***p<0.001; ****p<0.00001 c) Immunohistochemical stainings for S100 and STK11 were performed on two tissue micro arrays (TMA) of human primary melanoma tumors (N=166), of non-cranial (N=82) and on brain metastases (N=70). Scale bar = 300µm. d) Quantification of melanoma STK11+ cells was performed by QuPath. The average of 10 areas was calculated and normalized to S100. One-way Anova was used for statistical analysis *p<0.05; **p<0.01; ***p<0.001; ****p<0.00001

Figure 5. STK11 Loss Enhanced Activation of STAT3/5 and FAK

a) A human phospho-kinase array was performed on M990922 SCR and STK11-KO at 24h both under vehicle (DMSO) and LGX 20nM treatment. b) Comparative analysis of the vehicle treated cells. One-way Anova was used for statistical analysis. *p<0.05; **p<0.01; ***p<0.001 c) Confirmation of differential STAT3/5- and FAK-phosphorylation by WB in both BRAF and NRAS cells. d) Comparative analysis of vehicle treated cells with LGX-treated cells. Two-way Anova was used for statistical analysis. *p<0.05; **p<0.01; ***p<0.001

Figure 6. STK11 Loss-Mediated Invasion Is Prevented by STAT3/5- and FAK-inhibition

a) Collagen-embedded spheroids were treated with STAT3/5 (SH-45-4 and C188-9) and FAK (PF-573228) -inhibitors at 5µM for M990922 and at 20µM (SH-45-a) and 10 µM (PF-573228) for WM793B. Scale bar = 500µm. b) 3 spheres/condition were used to calculate the area of

invasion. Two-way Anova was used for statistical analysis. *p<0.05; **p<0.01; ***p<0.001 c) Pooled analysis of M990922 and WM793 confirmed the suppressive effects of STAT3/5- and FAK-inhibitors (STAT3/5i and FAKi) on invasion. d) M130425 STK11 KO spheroids were treated with STAT3/5 (C188-9) and FAK (PF-573228) –inhibitors at 10 µM. 6 spheres/condition were used to calculate the area of invasion. Scale bar = 500µm. e) Graphical conclusion. STK11 knockout leads to a STAT3/5 and FAK-dependent increase of invasion that can be targeted, using STAT3/5i and FAKi.

SUPPLEMENTARY MATERIAL AND METHODS

Material and methods

Human primary melanoma cells were obtained from the URPP melanoma biobank Zurich (Mitchell.Levesque@usz.ch) or from the American Type Culture Collection (ATCC, https://www.lgcstandards-atcc.org/). M990922, M150536 (URPP biobank) and WM793B (ATCC) carried activating BRAFV600E-mutations and M130425 (URPP Biobank) carried activating NRASQ61R-mutations. Human melanoma cells were cultured in RPMI 1640 medium (Sigma, Cat.No. R0883-500ML) supplemented with heat-inactivated FBS (10%, Pan Biotech, Cat.No. P30-1902, Lot.No. P160605), L-Glutamine (2mM, Gibco, Cat.No. 25030-024), Sodium-Pyruvate (1 mM, Sigma, Cat.No. S8636) and Normocin-Antimicrobial reagent (1x, InvivoGen, Cat.No. ant-nr-1) in a cell culture incubator (37°C, 5% CO2, 95% relative Humidity). The HEK293T cells (ATCC, Cat. No. CRL-3216) were cultured in DMEM with L-Glutamine and Pyruvate (Gibco, Cat.No. 41966-029) supplemented with heat-inactivated FBS (10%, Pan Biotech, Cat.No. P30-1902, Lot.No. P160605) and Pen-Strep (1%, Sigma, Cat.No. P4333-100ML) The immortalized microvascular endothelial cell lines hMEC1 (ATCC, Cat.No. CRL-3243) and hCMEC/D3 (Millipore, Cat.No. SCC066) were cultured in EndoGro MV complete medium adapted for human microvascular endothelial cells (Millipore, Cat.No. SCME004) and substituted with fibroblast growth-factor basic protein (bFGF) (1ng/mL, Millipore, Cat.No. GF003). Passaging: Cells were detached by removing the cell culture medium, washing with PBS ph7.4 (Gibco, Cat.No. 100010-015) followed by incubation with 0.05% Trypsin-EDTA (Gibco, Cat.No. 25300-054) in the recommended amount for the used cell culture dish (37°C, 1-3min). The trypsin was blocked with the appropriate serum-containing cell culture medium.

Transgenic cell lines

Expression plasmid creation:

Knockout: To create transgenic knock-out cell lines of STK11, the Clustered Regularly Interspaced Short Palindromic Repeats (CRISPR) and CRISPR-associated protein-9 nuclease (CRISPR/Cas9) system was used. We used the LentiCRISPRv2GFP (provided by David Feldser (Walter et al., 2017), Addgene plasmid #82416) and followed the Zhang lab protocol(Shalem et al., 2014) for the single guide RNA (sgRNA) insertion into the LentiCRISPRv2GFP-plasmid. We used the following sequences for our sgRNAs that have been identified using the sgRNA design tool CHOPCHOP (https://chopchop.cbu.uib.no)(CHOPCHOP v3: expanding the CRISPR web toolbox beyond genome editing | Nucleic Acids Research | Oxford Academic, n.d.):

STK11 sgRNA1 (KO1) targeting STK11 exon 6 (GGGTCTGTACCCCTTCGAAG), STK11 sgRNA2 (KO2) targeting STK11 exon 5 (AGGCCGTTGGCAATCTCGGG), STK11 sgRNA3 (KO3) targeting STK11 exon 3 (GCTCATCGGCAAGTACCTGA), and a non-targeting scrambled sequence (SCR) sgRNA (GAACAGTCGCGTTTGCGACT). The process of the virus production and cell transduction will be described separately below.

Overexpression: We used the pMuLE system from Ian J Frew et al. (Albers et al., 2015) for the creation of our overexpression plasmids. For the STK11 overexpression (STK11 oe) plasmid, the pMuLE ENTR CMV mCherry L1-R5 plasmid (all pMuLE plasmids were kindly provided by Ian J Frew, Addgene plasmid #62148) was digested with KpnI and SalI. Using NEBuilder HiFi DNA Assembly Master Mix (NEB, Cat.No. E2621) according to protocol the open-reading frame (ORF) of STK11 including vector backbone ligation arms was inserted (sequence including ligation arms in italic:

*AGGGAGACCCAAGCTTGGTACCGGCACC*ATGGAGGTGGTGGACCCGCAGCAGCTGGG

CATGTTCACGGAGGGCGAGCTGATGTCGGTGGGTATGGACACGTTCATCCACCGCAT

CGACTCCACCGAGGTCATCTACCAGCCGCGCCGCAAGCGGGCCAAGCTCATCGGCA

AGTACCTGATGGGGGACCTGCTGGGGGAAGGCTCTTACGGCAAGGTGAAGGAGGTG

CTGGACTCGGAGACGCTGTGCAGGAGGGCCGTCAAGATCCTCAAGAAGAAGAAGTT

GCGAAGGATCCCCAACGGGGAGGCCAACGTGAAGAAGGAAATTCAACTACTGAGG

AGGTTACGGCACAAAAATGTCATCCAGCTGGTGGATGTGTTATACAACGAAGAGAA

GCAGAAAATGTATATGGTGATGGAGTACTGCGTGTGTGGCATGCAGGAAATGCTGG

ACAGCGTGCCGGAGAAGCGTTTCCCAGTGTGCCAGGCCCACGGGTACTTCTGTCAGC

TGATTGACGGCCTGGAGTACCTGCATAGCCAGGGCATTGTGCACAAGGACATCAAG

CCGGGGAACCTGCTGCTCACCACCGGTGGCACCCTCAAAATCTCCGACCTGGGCGTG

GCCGAGGCACTGCACCCGTTCGCGGCGGACGACACCTGCCGGACCAGCCAGGGCTC

CCCGGCTTTCCAGCCGCCCGAGATTGCCAACGGCCTGGACACCTTCTCCGGCTTCAA

GGTGGACATCTGGTCGGCTGGGGTCACCCTCTACAACATCACCACGGGTCTGTACCC

CTTCGAAGGGGACAACATCTACAAGTTGTTTGAGAACATCGGGAAGGGGAGCTACG

CCATCCCGGGCGACTGTGGCCCCCCGCTCTCTGACCTGCTGAAAGGGATGCTTGAGT

ACGAACCGGCCAAGAGGTTCTCCATCCGGCAGATCCGGCAGCACAGCTGGTTCCGG

AAGAAACATCCTCCGGCTGAAGCACCAGTGCCCATCCCACCGAGCCCAGACACCAA

GGACCGGTGGCGCAGCATGACTGTGGTGCCGTACTTGGAGGACCTGCACGGCGCGG

ACGAGGACGAGGACCTCTTCGACATCGAGGATGACATCATCTACACTCAGGACTTC

ACGGTGCCCGGACAGGTCCCAGAAGAGGAGGCCAGTCACAATGGACAGCGCCGGG

GCCTCCCCAAGGCCGTGTGTATGAACGGCACAGAGGCGGCGCAGCTGAGCACCAAA

TCCAGGGCGGAGGGCCGGGCCCCCAACCCTGCCCGCAAGGCCTGCTCCGCCAGCAG

CAAGATCCGCCGGCTGTCGGCCTGCAAGCAGCAGTAA*GTCGACAATCCTCGAGCATG C*, ordered at IDT, custom sequence). The obtained CMV-STK11oe plasmid was recombined into the pMuLE Lenti Dest eGFP (Addgene plasmid #62175) together with pMuLE ENTR MCS L5-L2 (Addgene plasmid #62085) using the LR Clonase™ II Plus enzyme (ThermoFisher, Cat.No. 12538120) according to protocol.

For the empty vector (EV) plasmid, the two plasmids pMuLE ENTR MCS L1-R5 (Addgene plasmid #62084) and pMuLE ENTR MCS L5-L2 (Addgene plasmid #62085) were recombined into the pMuLE Lenti Dest eGFP (Addgene plasmid #62175).

Lentivirus production and cell transduction:

To produce the lentivirus necessary for the creation of the transgenic cell lines, 3.5*10^6 HEK293T cells were seeded into a 10cm dish for transfection with the viral plasmids. After 24h, each of the altered LentiCRISPRv2GFP expression plasmid now containing STK11 sgRNA 1, 2 or 3 or SCR sgRNA (4µg) was mixed with the packaging plasmid psPAX2 (2µg, provided by Didier Trono, Addgene plasmid #12260) and the envelope plasmid pMD2.G (1µg, provided by Didier Trono, Addgene plasmid #12259) and PEImax (21µg, Polysciences, Cat.No. 24765) in 1 mL of serum-free DMEM (Gibco, Cat.No. 11960-044) and incubated for 15 minutes at RT. The DNA/PEImax mixture was then added dropwise to the HEK293T cells. 24h post-transfection the medium was exchanged with 20mL HEK293T cell culture medium. This virus-containing medium was collected after 48h and sterile filtered using a 0.2 µm sterile filter to remove any residual HEK293T cells. For transduction, 100µL of the virus-containing medium were added

together with polybrene (8µg/mL) to the requested cells that were 80% confluent in a 6-well. GFP-positive cells were sorted as single cells into a 96-well plate by the FACSAria™ III fluorescence-activated cell sorter (BD Biosciences), raised and assessed for successful knock-out.

Cellular Assays

Colorimetric Resazurin-based viability assay:

Cells were seeded into 96-well plates and treated 1d post-seeding for 72h and/or 144h with LGX818 (Selleckchem, Cat.no. S7108), AICAR (Selleckchem, Cat.No. S1802) or the combination thereof in the stated concentrations. Triplicates were seeded for each condition. For the IC50-evaluation against LGX818, different wells were treated with ascending concentrations of the drug. At the day of assessment, the medium was exchanged with cell-culture medium containing Resazurin sodium salt (0.015mg/mL, Sigma-Aldrich, Cat.No. R7017) and incubated for 1.5h (37°C). The amount of metabolized fluorescent resorufin, which correlates with the amount of living cells was read at 535nm excitation and 595 emission.

Colony formation assay:

Cells were seeded in 12-well plates and treated with LGX for the indicated duration. Medium was changed every 72h. To assess the colonies the cells were fixed and stained with a filtered crystal violet solution (Crystal violet 0.05%w/v, Formaldehyde 1%, Methanol 1%, in PBS) for 20min at room temperature and washed with water. The plates were air-dried, scanned and analyzed using the ImageJ plug-in ColonyArea as previously described (Guzmán et al., 2014).

3D-multicellular spheroid assay and spheroid collagen invasion assay:

To inhibit the cells from adhering to the bottom of the cell culture dish, but form 3D-multicellular spheroids instead, 96-well plates had to be precoated by incubating 50 µL per well of 1.5%w/v noble agar (Difco, Cat.No. 5308689) solubilized in base RPMI (Sigma, Cat.No.

R0883) for 1h at room-temperature and under ultraviolet iradiation. Per well 4000 cells were seeded and incubated at 37°C until they formed compact spheroids (3-4 days).

The formed spheroids were either treated directly for drug response assessment or embedded into 60 µL of a collagen I-mixture in a novel noble-agar precoated 96-well, to evaluate collagen-invasion capabilities with or without treatment. In any case, the medium (with or without treatment) was exchanged every 72h. The collagen I-mixture consisted of 2.3 mL type I rat tail collagen (Corning, Cat.No. 354236) adjusted to 3.3 mg/mL with 0.02N acetic acid, 570 µL DMEM (Gibco, Cat.No. 11960-044), 25 µL L-Glutamine (Gibco, Cat.No. 25030-024), 30 µL FCS (company, Cat.No.) and 60 µL of 7.5% Sodium-Bicarbonate in PBS. To avoid preliminary polymerization, the collagen-mix was never prepared in larger amounts and always on ice. The spheroids were photographed over a period of 12-14d. The spheroids were photographed over a period of 12-14d. Live/dead fluorescent staining was performed with a staining solution of serum-free RPMI with 8 µM calcein AM (live) (Sigma, Cat.No. 17783) and 10 µM ethidium homodimer (death) (Sigma, Cat.No. 46043). The spheres were assessed by 8 µM calcein AM (live) (Sigma, Cat.No. 17783) and 10 µM ethidium homodimer (death) stain (Sigma, Cat.No. 46043).

Collagen-adhesion assay:

Prior to the adhesion assays the melanoma cell lines were starved with RPMI complete with 1% FCS overnight. On the day of the assay, 96-well plates were coated with rat-tail collagen type 1 (100 µg/mL) diluted in PBS and incubated at 37°C for 1h. The plates were then washed with PBS and blocked with blocking buffer (serum-free DMEM (Gibco, Cat.No. 11960-044) with 0.5% BSA (Sigma, Cat.No. A7906), to block any remaining plastic at 37°C for at least 60min. After removal of the blocking buffer, 20’000 cells in 100 µL serum-free cell culture medium

were added to each well and incubated for the indicated time. Non-adherent cells were removed by washing three times with PBS. The cells were then fixed and stained with a filtered crystal violet solution (Crystal violet 0.05%w/v, Formaldehyde 1%, Methanol 1%, in PBS) for 20min at room temperature and washed three times with water. After air-drying of the plates, the crystal violet was solubilized through incubation with 100 µL SDS 2% (20% stock from Rockland, Cat.No. MB-046-1000) per well at room temperature for 30min while shaking. The absorbance was read at 550nm

Endothelial-cell adhesion assay:

The immortalized microvascular endothelial cells hMEC1 and hCMEC/D3 were seeded into a corning 4-well chamber slide (Falcon, Cat.No. 354114) (25'000 cells per 1.7cm^2 chamber) and grown to 100% confluency (ca 4d). Prior to the adhesion assays the melanoma cell lines were starved with RPMI complete with 1% FCS overnight. On the day of the assay, the cells were detached with trypsin, resuspended in serum-containing medium, washed with PBS and stained with the fluorescent dye Vybrant DiI (1 µg/mL, ThermoFisher, Cat.No. V22885) in serum-free RPMI for 30min at 37°C. The stained cells were then centrifuged, washed, seeded into the chambers (50'000 cells per 1.7cm^2 chamber) in serum-free RPMI and incubated at 37°C for the indicated amount of time. The slides were then washed three times with PBS and fixed with 4% formaldehyde for 20 min at room-temperature. The chambers were then removed and the slides covered with glycerol 50% v/v in PBS and a cover slip. Per well, 5 pictures were taken at 20x, and the fluorescent cells were counted.

Immunostainings

Immunoblot: Cells were detached by trypsin, resuspended in serum-containing cell culture medium, washed with cold PBS and lysed by snap-freezing at -80°C for 30min in cell lysis buffer. The cell lysis buffer contained the following components: NaCl 150mM, MgCl2 15mM, EGTA 1mM, Hepes 50mM, Glycerol 10%, Triton-X 1% solved in ddH2O and the pH adjusted to 7.5. The buffer was supplemented with the phosphatase inhibitor cocktail PhosSTOP EASYpack (1 tablet per 10mL, Roche, Cat.No 05892970001) and protease inhibitor cOmplete ULTRA Tablets (1 tablet per 10mL, Roche, Cat.No 04906845001). The remaining cell debris was centrifuged (4°C, 21'000 rcf, 15min) and the protein-containing supernatant was collected and standardized to equal amounts. We used the following antibodies for immunoblots, some of which were also used for immunohistochemical stains if not stated otherwise: STK11 (CST #3047), ERK1/2 (CST #4695), p-ERK1/2 T202/Y204 (CST# 4376), STAT3 (CST #9132), p-STAT3 Y705 (#9138), p-STAT3 S727 (CST #9134), FAK (CST #3285), p-FAK Y397 (CST #3283), p-STAT5A/B Y699/Y694 (CST #9359S) For immunohistochemical stainings, the cool IHC machine was used! We used Dako Target Retrieval Solution pH9 for all stainings. The following antibodies were used specifically for IHC: STK11 (SantaCdruz, Cat.No. sc-374334), S100 (Novocastra, Cat.No. NCL-L-S100).

The TMAs with melanoma primary tumors (TMA18 and TMA19) were a gift from the URPP biobank Zurich, University Hospital Zurich, Switzerland (Mitch Levesque). The TMA with melanoma metastases from different origins was purchased from Biomax (Cat.No. BCC38218). The brain metastasis TMA was a gift from Ruth Lyck, University of Bern, Switzerland. TMA analysis was performed with QuPath, closely following the "QuPath TMA CD3 analysis" manual on github (https://github.com/qupath/qupath/wiki/TMA-CD3-analysis).

Human Phospho-Kinase Array Kit

The Proteome Profiler Human Phospho-Kinase Array Kit (R&D systems, Cat. No. ARY003B) was used. 2.5 Mio cells were seeded into a T175 flask and treated with LGX (20nM) or DMSO 48h after seeding for another 24h. Per condition, 5.0 Mio cells were lysed in 0.5mL of the kit lysis buffer. The protein was lysed, and each sample was adjusted to 600ng before following the kit instruction. The exposed blots were analyzed using ImageJ by measuring and averaging each dot. A two-tailed Student's T-test was performed by analyzing different exposure times of the same membranes.

Zebrafish husbandry

Zebrafish xenograft experiments were performed in collaboration with Professor Natascia Tiso at the zebrafish facility of the University of Padova, Italy. Zebrafish strains were maintained according to standard procedures (Westerfield, 2000).

Zebrafish xenografts

For the injection, the cells were detached with trypsin, resuspended in serum-containing cell culture medium, washed with PBS and stained with the fluorescent dye Vybrant DiI (1 µg/mL, ThermoFisher, Cat.No. V22885) in serum-free RPMI for 30 min at 37°C. The stained cells were then centrifuged, washed with PBS and resuspended in serum-free RPMI at a concentration of 1x10^6 cells per 10 µL. The cells were injected into zebrafish embryos at 2 days post-fertilization (dpf). Immediately before xenografting the cells, the embryos were anesthetized with a solution of tricaine (160 mg/L; Sigma-Aldrich, Cat. No. A5040), embedded in 2% (w/v) methylcellulose (Sigma-Aldrich, Cat.No. A9414) in fish water (150 mg/L Instant Ocean, 6.9

mg/L NaH2PO4, 12.5 mg/L Na2HPO4, pH 7.2) and mounted on a custom-made multi-lane plastic support. The cells were injected into the yolk as a single droplet (100 µm diameter, about 100 cells/embryo), using a WPI microinjector. At 1-day post injection (dpi), the fish were assessed for successful yolk-injection and kept in fish water with either DMSO or the BRAFi LGX818 at 10 nM until 6dpi. The cells were then fixed and assessed for fluorescent-positive metastasis formation under fluorescence microscopy (Leica M165 FC microscope with DFC7000T camera).

SUPPLEMENTARY FIGURES AND LEGENDS

Figure S1 Evaluation of STK11 constructs viability.

a) Transgenic cell line generation. For all cell cultures, a monoclonal cell line was created. These cell lines were transduced with SCR (non-targeting sgRNA), STK11-KO1, STK11-KO2 and STK11-KO3 sgRNA/Cas9 constructs. For each cell line, one SCR and two KO-clones were amplified. b) and c) MTT assay of STK11 SCR vs STK11-KO. Data represent the mean ± S.D. of triplicate determinations. Two-way Anova was used for statistical analysis *p<0.05; **p<0.01; ***p<0.001; ****p<0.00001 d) 2000 cells (M990922) and 3000 cells (WM793B and M130425) were seeded in 96-well plates and 2D MTT viability assay was performed over time e) 3D multicellular cells successfully formed 4d after seeding 4000 cells per well into an agarose coated 96 well plate. Scale bar = 500µm.

Figure S2 Evaluation of STK11 expression upon BRAF- inhibition.

a) IC50-values of the BRAFi-sensitive melanoma cells and their matched BRAFi-resistant counterparts. b) Western Blot (left) with densitometry (right) of BRAFi-sensitive (S) cell lines and their matched BRAFi-resistant (R) counterparts after continuously exposing them to LGX (100nM).

Figure S3 Evaluation of sensitivity to BRAFi in SCR vs STK11-KO melanoma cells in 3D models.

a) Collagen-embedded spheroids were treated with LGX 50nM for 7d and 16d. Scale bar = 500µm. b) 3 spheres/condition were used to calculate the area of invasion. Two-way Anova was used for statistical analysis. *p<0.05; **p<0.01; ***p<0.001 c) 3D spheres were treated with LGX for 16d and viability was evaluated by Calcein-AM/Ethidium homodimer staining. Scale bar = 1000µm. Live/dead ratio was quantified with Photoshop. 6 spheres/condition were quantified. Two-way Anova was used for statistical analysis. *p<0.05; **p<0.01; ***p<0.001, ****p<0.00001

Figure S4 STK11 is inversely correlated with invasion.

a) WB of M150536 EV compared to STK11oe. b) Brightfield images of representative collagen embedded M150536 EV spheroids versus M150536 STK11oe spheroids after 6d. Scale bar = 500µm.

Figure S5 Evaluation of metastasis formation in SCR vs STK11-KO injected zebrafish larvae.

a) The yolk of 2d old Zebrafish larvae was injected with human melanoma cell lines and assessed on the next day (1dpi) for successful injection, before treatment start. Scale bar = 1000µm. b) The survival of the embryos under vehicle and LGX treatment, was assessed until 6d. c) and d) At 6d post-transplantation under vehicle and LGX treatment, the injected fish were assessed for fluorescently labeled metastases outside the yolk for both, M990922 and WM793B by a blind investigator. d) Evaluation of brain metastasis in SCR and STK11-KO injected zebrafish

Figure S6 The overexpression of STK11 or the treatment with STAT3/5i and/or FAKi reverts the invasive phenotype of STK11-KO spheres.

a) WB of STAT3, STAT5a/b- and FAK-phosphorylation in M150536 EV compared to STK11 oe. b-c) M990922 and WM793B were treated with increasing concentrations of STAT3/5 (SH-45-4 and C188-9) and FAK (PF-573228) –inhibitors alone or in combination. After 16d the viability of the spheres was assessed by Calcein-AM/Ethidium homodimer staining. Scale bar = 1000µm (b) and 750µm (c). d) 6 spheres per condition were used to calculate the area of invasion. Two-way Anova was used for statistical analysis. *p<0.05; **p<0.01; ***p<0.001; ****p<0.00001

Figure S7 Treatment with STAT3/5i and/or FAKi reverts the invasive phenotype of STK11-KO spheres in NRAS STK11-KO.

a) M130425 STK11-KO spheroids were treated with increasing concentrations of STAT3/5 (C188-9) and FAK (PF-573228) –inhibitors alone or in combination. After 9 days the viability of the spheres was assessed by Calcein-AM/Ethidium homodimer staining. Scale bar = 500µm. b) 6 spheres/condition were used to calculate the area of invasion. Two-way Anova was used for statistical analysis. *p<0.05; **p<0.01

SUPPLEMENTARY TEXT REFERENCES

Albers J, Danzer C, Rechsteiner M, Lehmann H, Brandt LP, Hejhal T, et al. A versatile modular vector system for rapid combinatorial mammalian genetics. J Clin Invest 2015;125:1603–19. https://doi.org/10.1172/JCI79743.

CHOPCHOP v3: expanding the CRISPR web toolbox beyond genome editing | Nucleic Acids Research | Oxford Academic. n.d. https://academic.oup.com/nar/article/47/W1/W171/5491735 (accessed September 24, 2020).

Guzmán C, Bagga M, Kaur A, Westermarck J, Abankwa D. ColonyArea: An ImageJ Plugin to Automatically Quantify Colony Formation in Clonogenic Assays. PLOS ONE 2014;9:e92444. https://doi.org/10.1371/journal.pone.0092444.

Shalem O, Sanjana NE, Hartenian E, Shi X, Scott DA, Mikkelsen TS, et al. Genome-Scale CRISPR-Cas9 Knockout Screening in Human Cells. Science 2014;343:84–7. https://doi.org/10.1126/science.1247005.

Vito G de, Vito G de, Ricci P, Turrini L, Turrini L, Gavryusev V, et al. Effects of excitation light polarization on fluorescence emission in two-photon light-sheet microscopy. Biomed Opt Express 2020;11:4651–65. https://doi.org/10.1364/BOE.396388.

Walter DM, Venancio OS, Buza EL, Tobias JW, Deshpande C, Gudiel AA, et al. Systematic In Vivo Inactivation of Chromatin-Regulating Enzymes Identifies Setd2 as a Potent Tumor Suppressor in Lung Adenocarcinoma. Cancer Res 2017;77:1719–29. https://doi.org/10.1158/0008-5472.CAN-16-2159.

Westerfield M. The zebrafish book. A guide for the laboratory use of zebrafish (Danio rerio). 4th ed. Eugene, Oregon: University of Oregon Press; 2000.

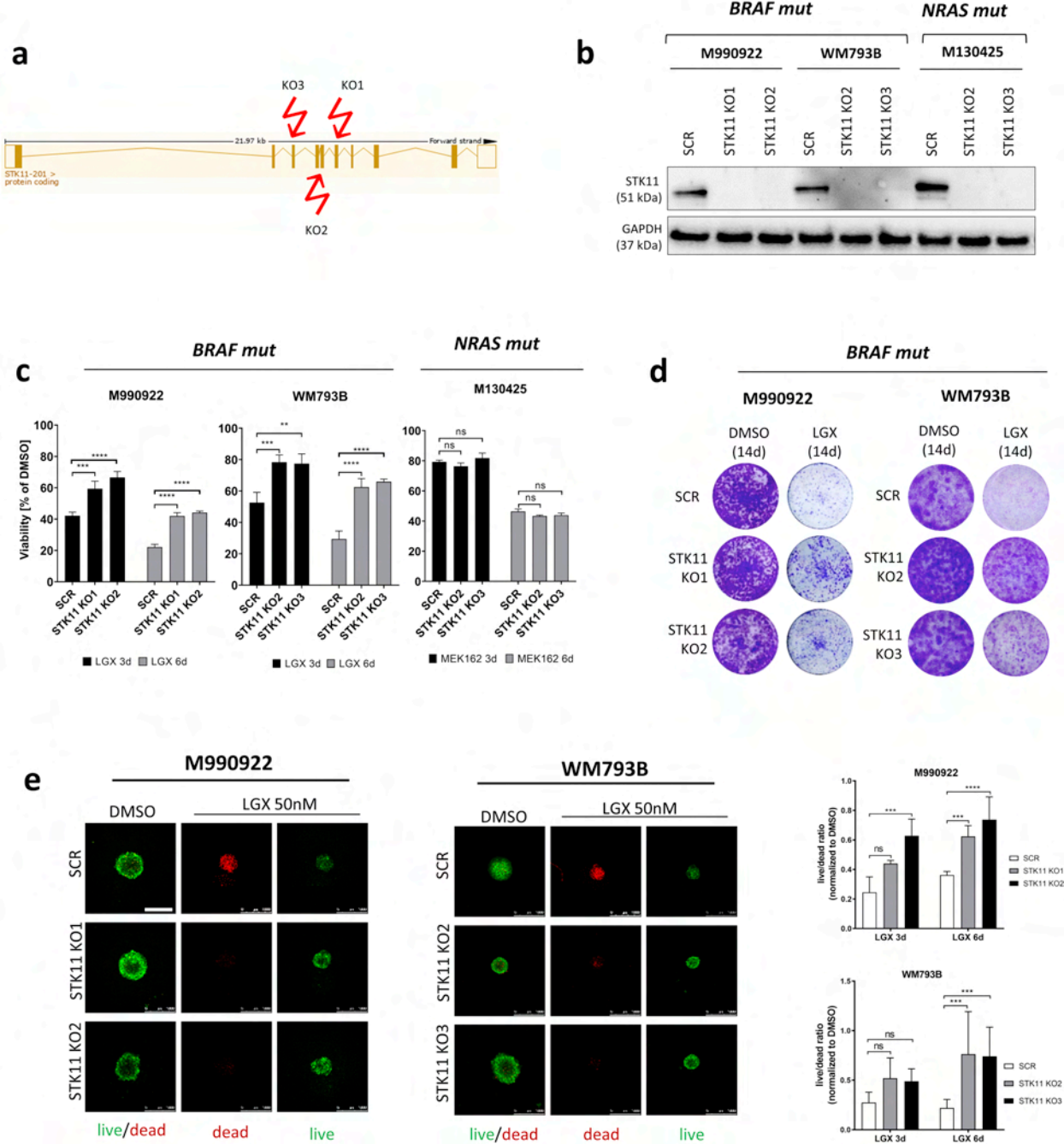
a
KO3
KO1
KO2
21.97 kb
Forward strand
STK11-201 > protein coding
b
BRAF mut
NRAS mut
M990922
WM793B
M130425
SCR
STK11 KO1
STK11 KO2
STK11 KO3
STK11 (51 kDa)
GAPDH (37 kDa)
c
BRAF mut
NRAS mut
M990922
WM793B
M130425
Viability [% of DMSO]
LGX 3d
LGX 6d
MEK162 3d
MEK162 6d
d
BRAF mut
M990922
WM793B
DMSO (14d)
LGX (14d)
SCR
STK11 KO1
STK11 KO2
STK11 KO3
e
M990922
WM793B
DMSO
LGX 50nM
SCR
STK11 KO1
STK11 KO2
STK11 KO3
live/dead
dead
live
live/dead ratio (normalized to DMSO)
LGX 3d
LGX 6d

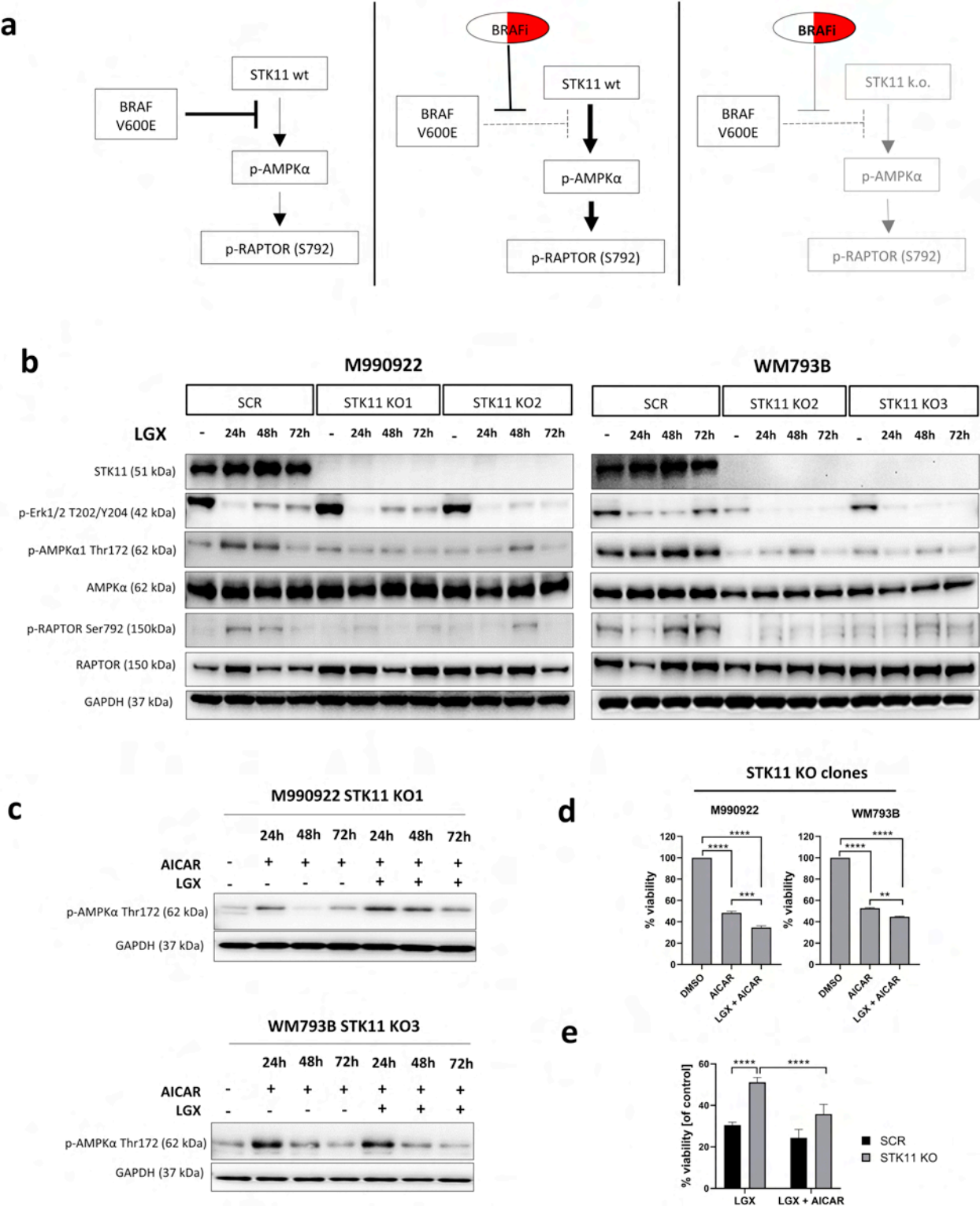
a
BRAF V600E
STK11 wt
p-AMPKα
p-RAPTOR (S792)
BRAFi
BRAF V600E
STK11 wt
p-AMPKα
p-RAPTOR (S792)
BRAFi
BRAF V600E
STK11 k.o.
p-AMPKα
p-RAPTOR (S792)
b
M990922
WM793B
SCR
STK11 KO1
STK11 KO2
STK11 KO3
LGX
- 24h 48h 72h
STK11 (51 kDa)
p-Erk1/2 T202/Y204 (42 kDa)
p-AMPKα1 Thr172 (62 kDa)
AMPKα (62 kDa)
p-RAPTOR Ser792 (150kDa)
RAPTOR (150 kDa)
GAPDH (37 kDa)
c
M990922 STK11 KO1
24h 48h 72h 24h 48h 72h
AICAR
LGX
p-AMPKα Thr172 (62 kDa)
GAPDH (37 kDa)
WM793B STK11 KO3
24h 48h 72h 24h 48h 72h
AICAR
LGX
p-AMPKα Thr172 (62 kDa)
GAPDH (37 kDa)
d
STK11 KO clones
M990922
WM793B
% viability
DMSO
AICAR
LGX + AICAR
e
% viability [of control]
LGX
LGX + AICAR
SCR
STK11 KO

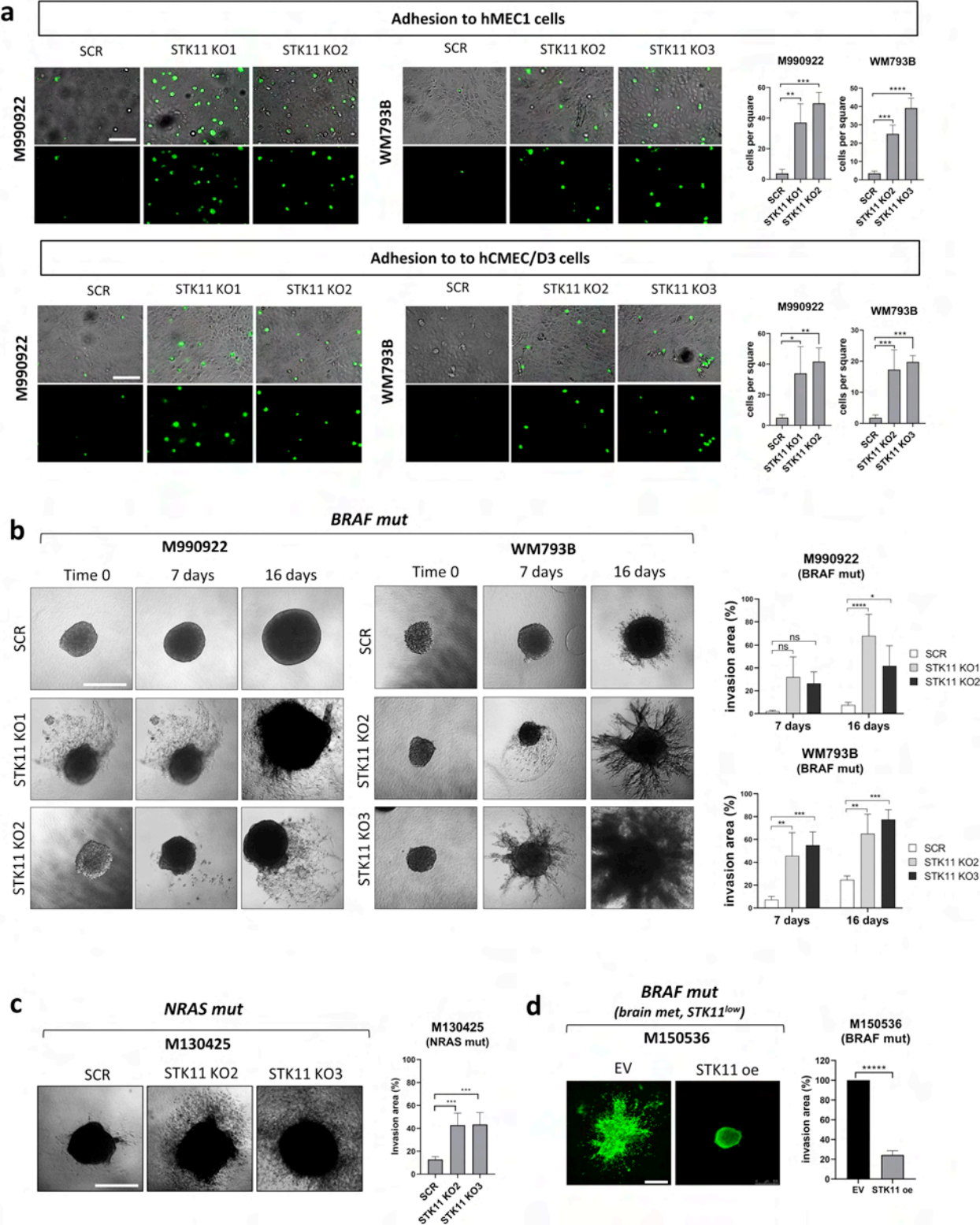
a
Adhesion to hMEC1 cells
SCR
STK11 KO1
STK11 KO2
STK11 KO3
M990922
WM793B
cells per square
Adhesion to to hCMEC/D3 cells
b
BRAF mut
Time 0
7 days
16 days
STK11 KO1
STK11 KO2
STK11 KO3
invasion area (%)
c
NRAS mut
M130425
(NRAS mut)
d
BRAF mut
(brain met, STK11low)
M150536
EV
STK11 oe
(BRAF mut)

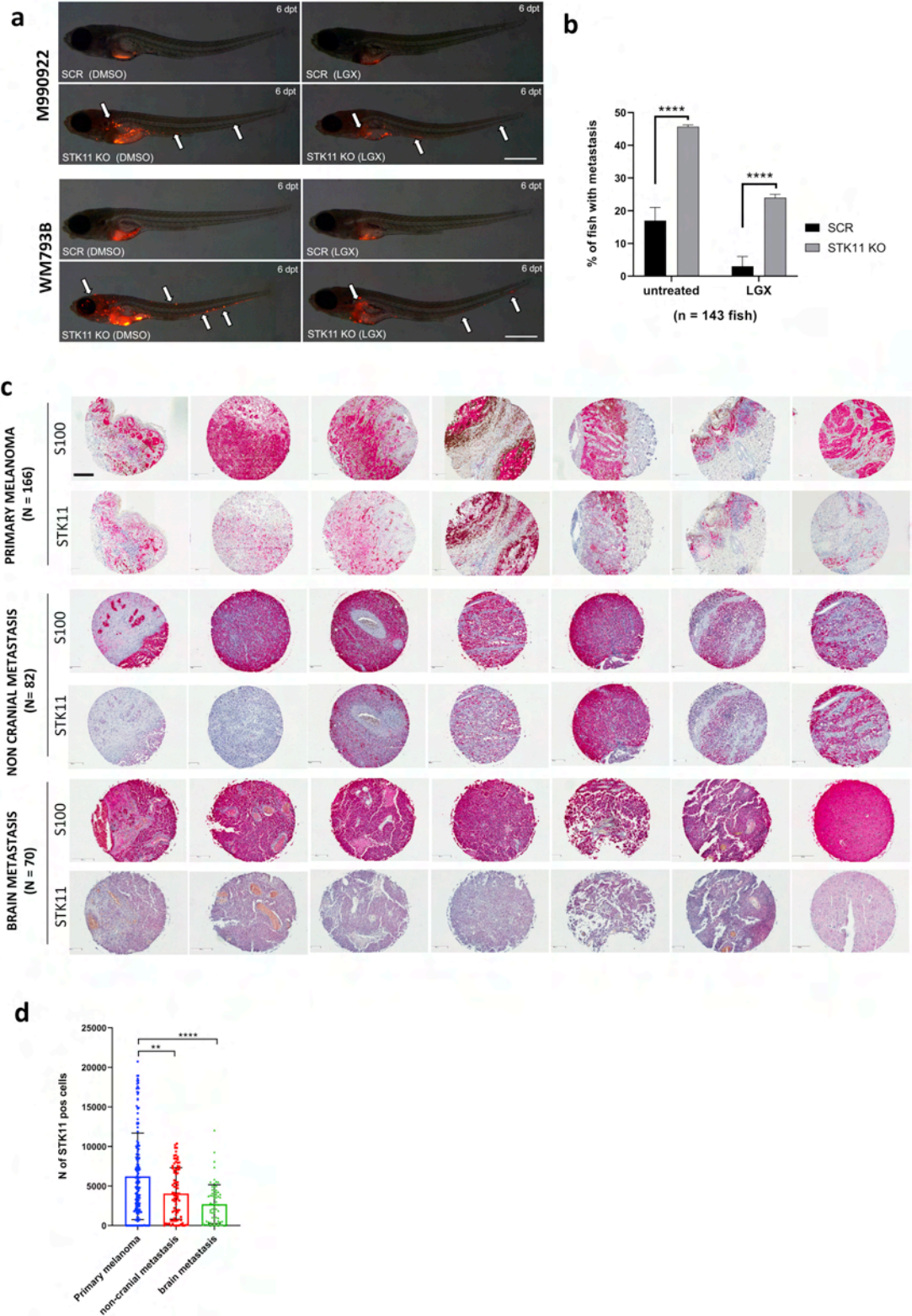
a
M990922
WM793B
6 dpt
SCR (DMSO)
SCR (LGX)
STK11 KO (DMSO)
STK11 KO (LGX)
b
% of fish with metastasis
****
****
SCR
STK11 KO
untreated
LGX
(n = 143 fish)
c
PRIMARY MELANOMA (N = 166)
NON CRANIAL METASTASIS (N= 82)
BRAIN METASTASIS (N = 70)
S100
STK11
d
N of STK11 pos cells
**
****
Primary melanoma
non-cranial metastasis
brain metastasis

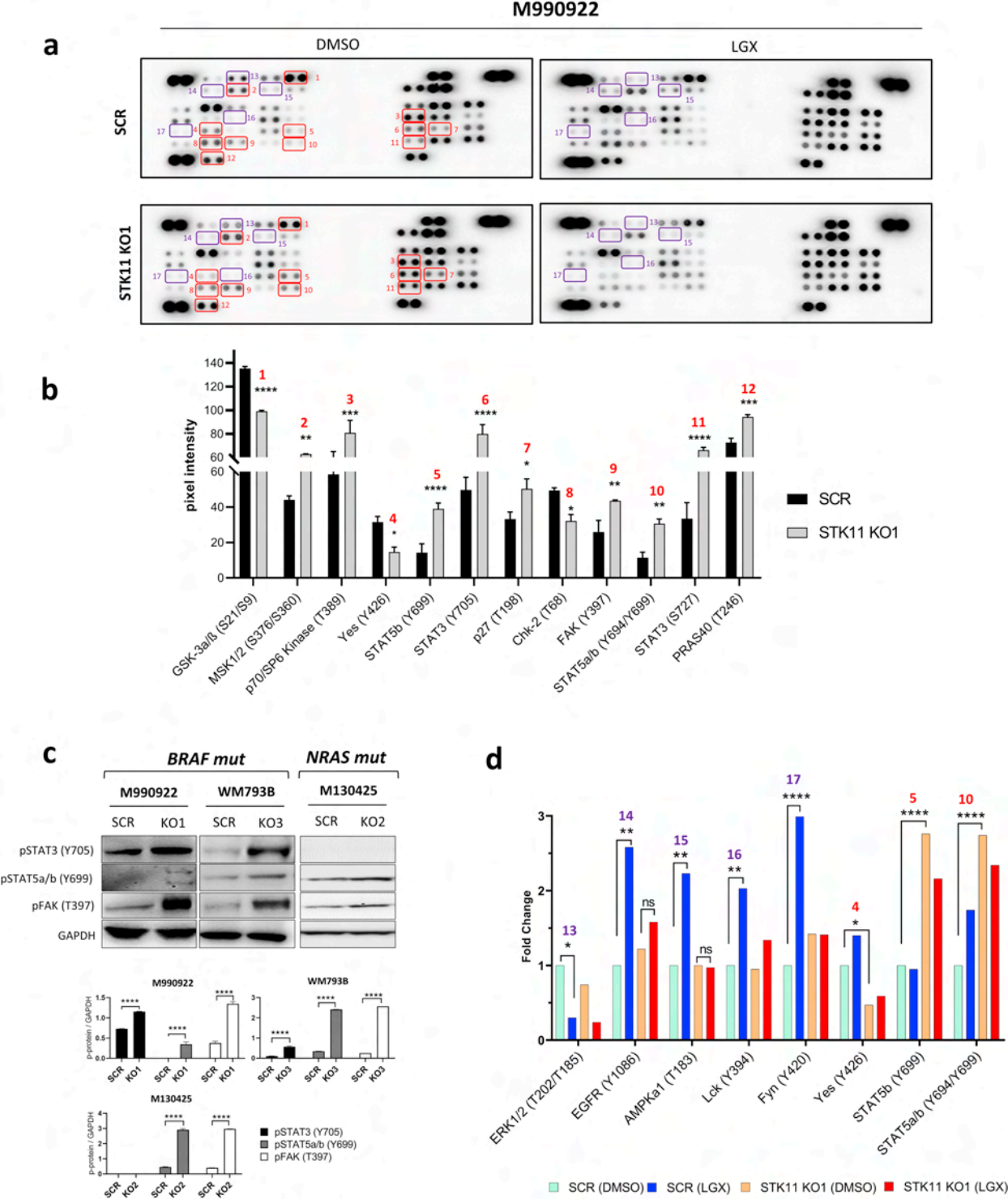
M990922
a
DMSO
LGX
SCR
STK11 KO1
b
pixel intensity
SCR
STK11 KO1
GSK-3a/ß (S21/S9)
MSK1/2 (S376/S360)
p70/SP6 Kinase (T389)
Yes (Y426)
STAT5b (Y699)
STAT3 (Y705)
p27 (T198)
Chk-2 (T68)
FAK (Y397)
STAT5a/b (Y694/Y699)
STAT3 (S727)
PRAS40 (T246)
c
BRAF mut
NRAS mut
M990922
WM793B
M130425
SCR
KO1
KO3
KO2
pSTAT3 (Y705)
pSTAT5a/b (Y699)
pFAK (T397)
GAPDH
p-protein / GAPDH
d
Fold Change
ERK1/2 (T202/T185)
EGFR (Y1086)
AMPKa1 (T183)
Lck (Y394)
Fyn (Y420)
Yes (Y426)
STAT5b (Y699)
STAT5a/b (Y694/Y699)
SCR (DMSO)
SCR (LGX)
STK11 KO1 (DMSO)
STK11 KO1 (LGX)

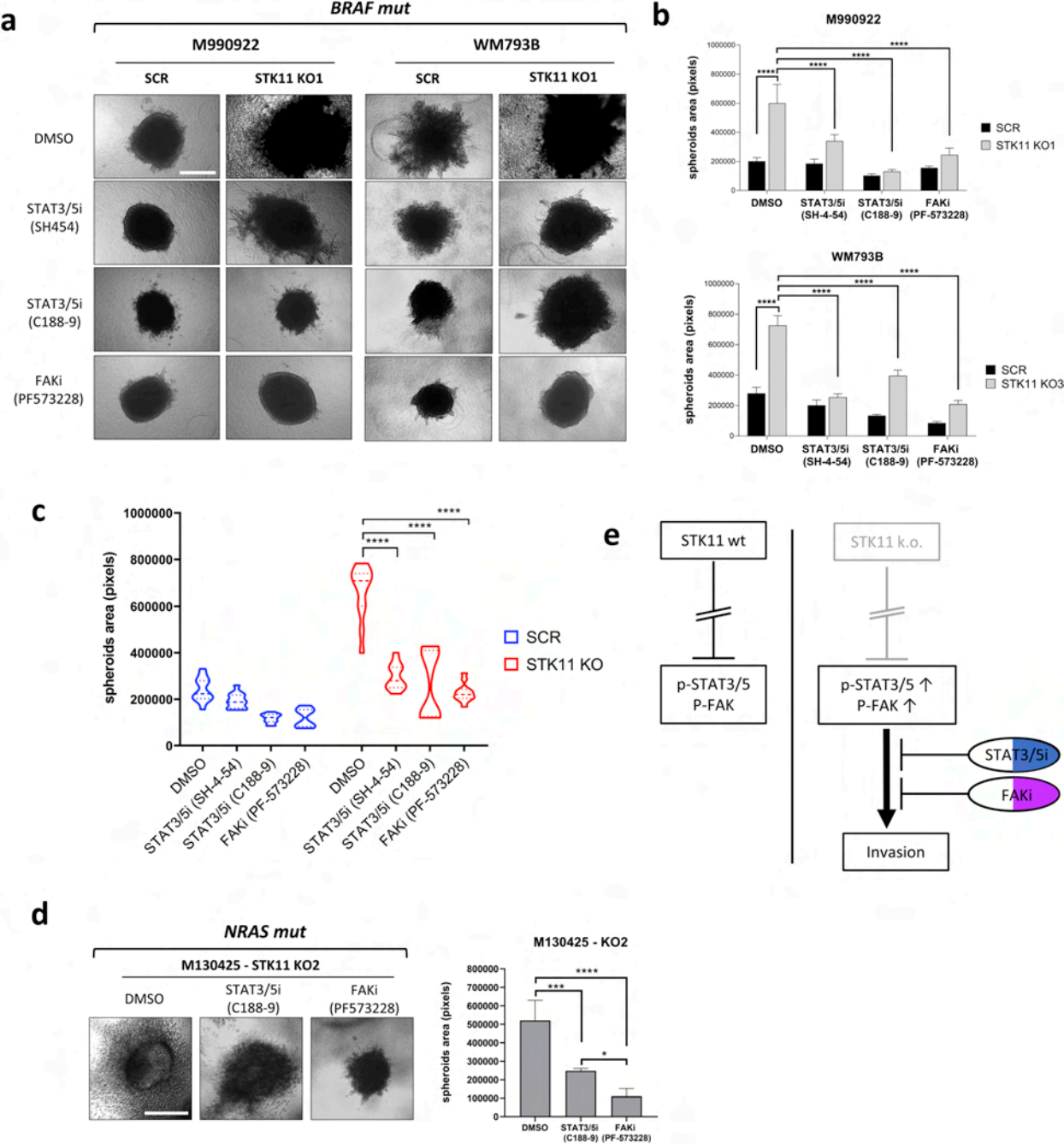
a
BRAF mut
M990922
WM793B
SCR
STK11 KO1
SCR
STK11 KO1
DMSO
STAT3/5i (SH454)
STAT3/5i (C188-9)
FAKi (PF573228)
b
M990922
spheroids area (pixels)
SCR
STK11 KO1
DMSO
STAT3/5i (SH-4-54)
STAT3/5i (C188-9)
FAKi (PF-573228)
WM793B
spheroids area (pixels)
SCR
STK11 KO3
DMSO
STAT3/5i (SH-4-54)
STAT3/5i (C188-9)
FAKi (PF-573228)
c
spheroids area (pixels)
SCR
STK11 KO
DMSO
STAT3/5i (SH-4-54)
STAT3/5i (C188-9)
FAKi (PF-573228)
DMSO
STAT3/5i (SH-4-54)
STAT3/5i (C188-9)
FAKi (PF-573228)
d
NRAS mut
M130425 - STK11 KO2
DMSO
STAT3/5i (C188-9)
FAKi (PF573228)
M130425 - KO2
spheroids area (pixels)
DMSO
STAT3/5i (C188-9)
FAKi (PF-573228)
e
STK11 wt
p-STAT3/5
P-FAK
STK11 k.o.
p-STAT3/5 ↑
P-FAK ↑
STAT3/5i
FAKi
Invasion

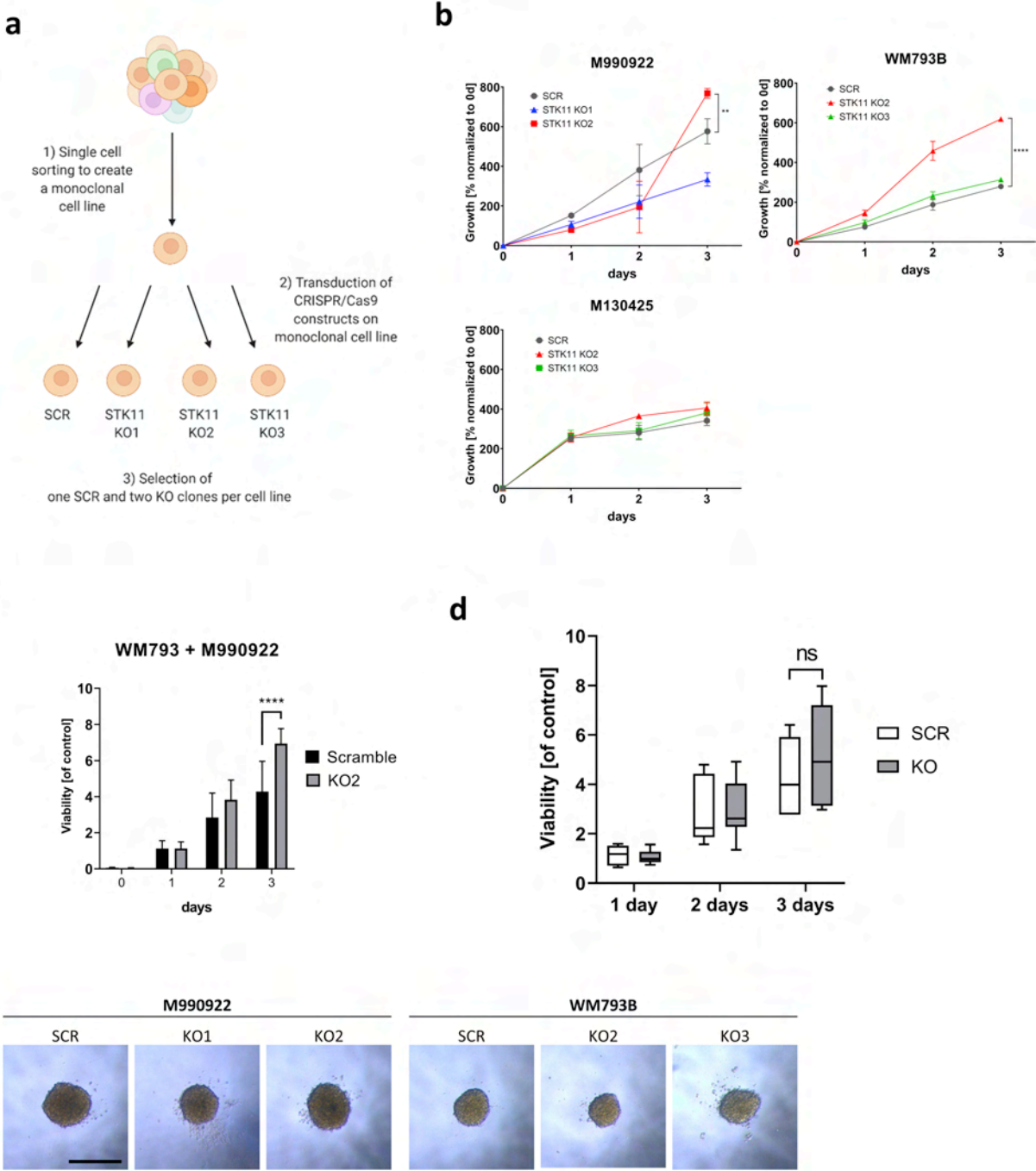
a
1) Single cell sorting to create a monoclonal cell line
2) Transduction of CRISPR/Cas9 constructs on monoclonal cell line
SCR
STK11 KO1
STK11 KO2
STK11 KO3
3) Selection of one SCR and two KO clones per cell line
b
M990922
WM793B
M130425
SCR
STK11 KO1
STK11 KO2
STK11 KO3
Growth [% normalized to 0d]
days
c
WM793 + M990922
Viability [of control]
Scramble
KO2
****
days
d
Viability [of control]
ns
SCR
KO
1 day
2 days
3 days
e
M990922
WM793B
SCR
KO1
KO2
KO3

a

CELL LINE	MUTATION	LGX IC50 [nM]
M990922-S	BRAFV600E	4
M990922-R	BRAFV600E	939
WM793B-S	BRAFV600E	3
WM793B-R	BRAFV600E	240
A375-S	BRAFV600E	3
A375-R	BRAFV600E	4127
SKMEL28-S	BRAFV600E	2
SKMEL28-R	BRAFV600E	1391
WM983A-S	BRAFV600E	45
WM983A-R	BRAFV600E	892

b

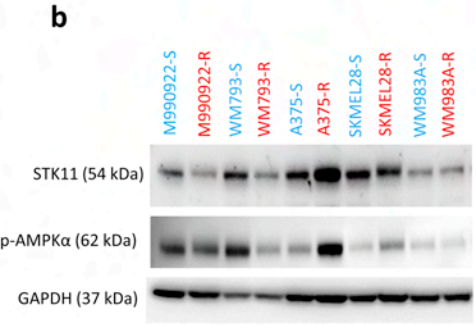

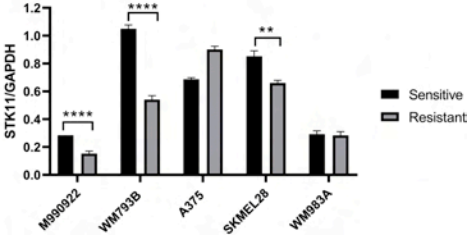

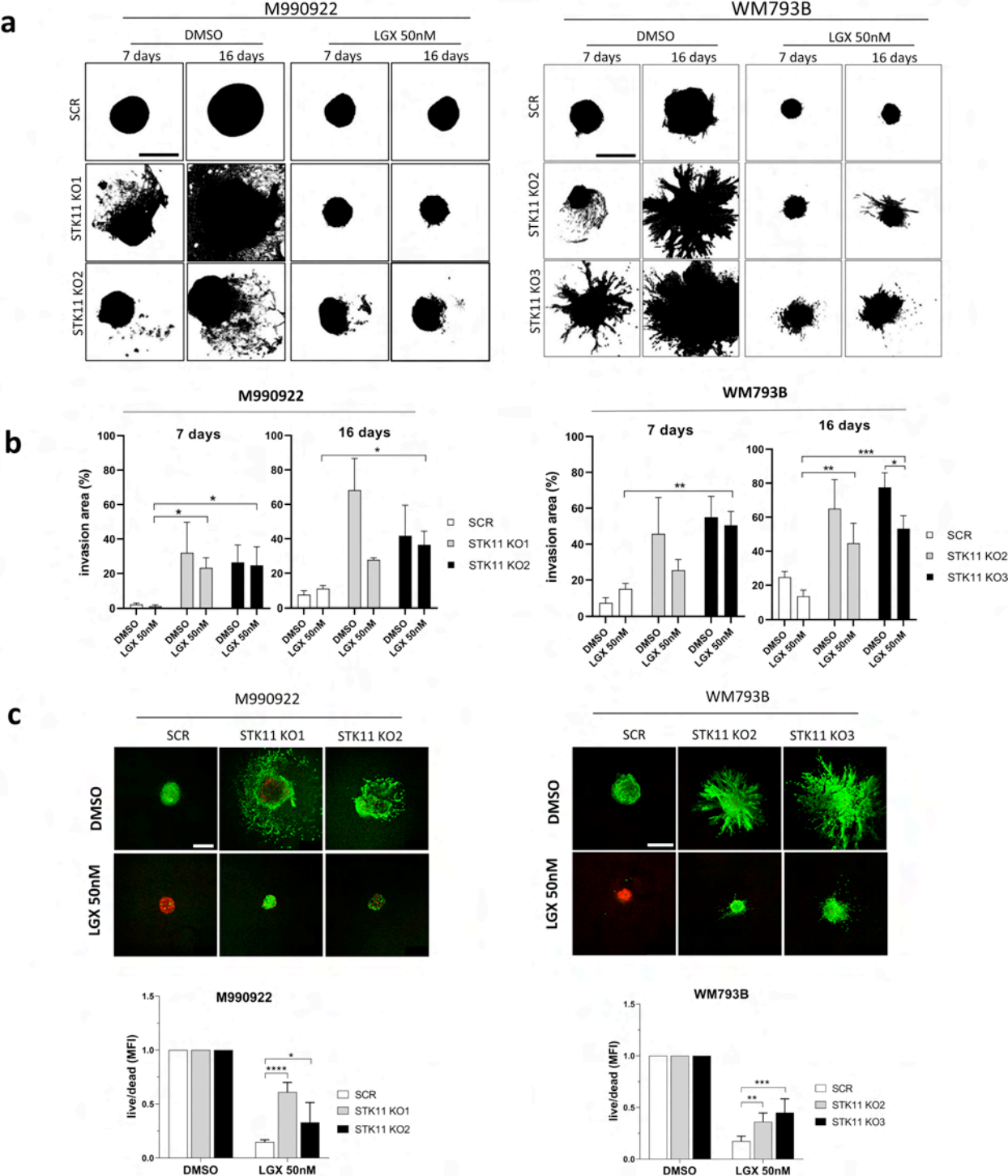
a
M990922
WM793B
DMSO
LGX 50nM
7 days
16 days
SCR
STK11 KO1
STK11 KO2
STK11 KO3
b
M990922
WM793B
7 days
16 days
invasion area (%)
SCR
STK11 KO1
STK11 KO2
STK11 KO3
DMSO
LGX 50nM
c
M990922
WM793B
SCR
STK11 KO1
STK11 KO2
STK11 KO3
DMSO
LGX 50nM
live/dead (MFI)

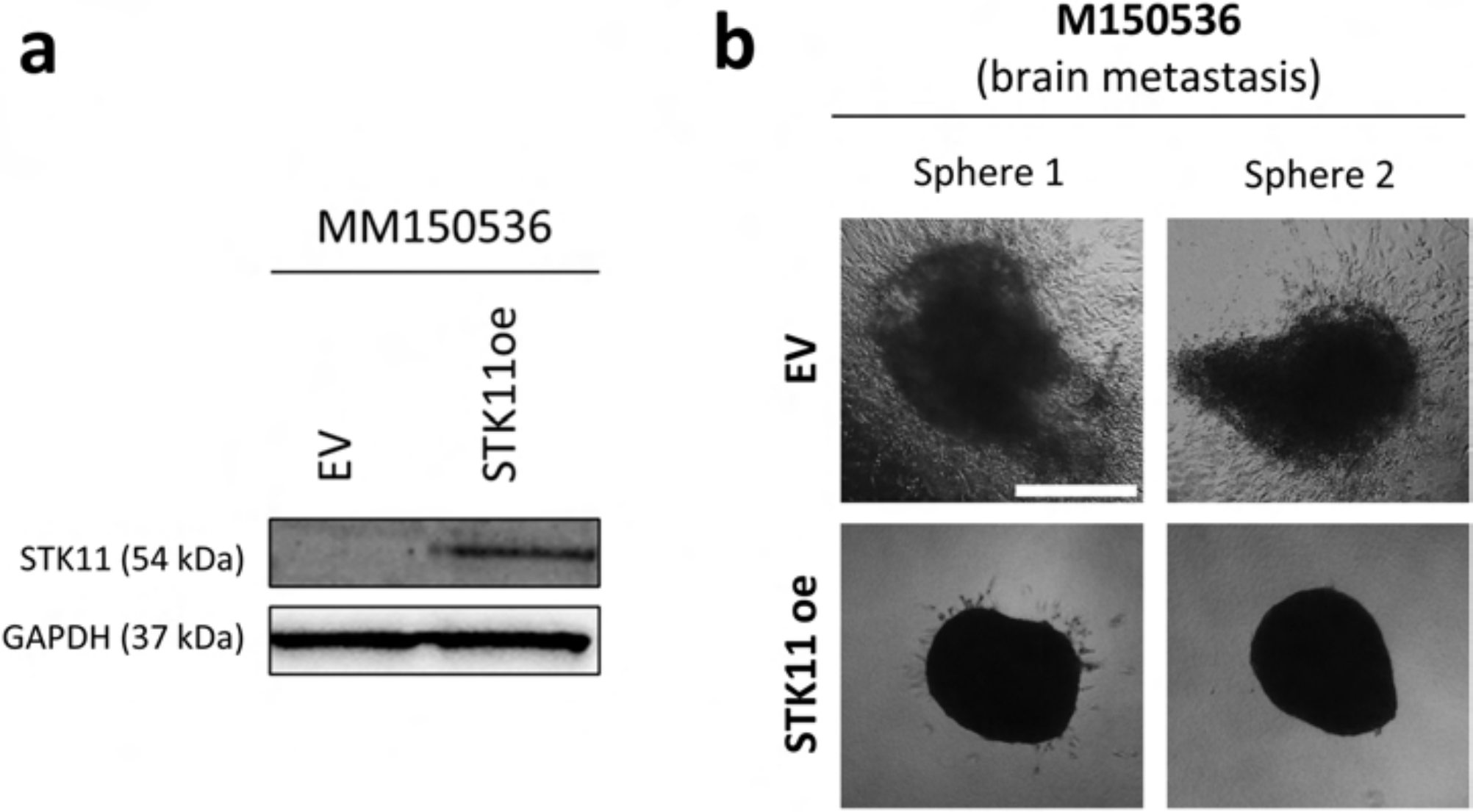
a
MM150536
EV
STK11oe
STK11 (54 kDa)
GAPDH (37 kDa)
b
M150536
(brain metastasis)
Sphere 1
Sphere 2
EV
STK11 oe

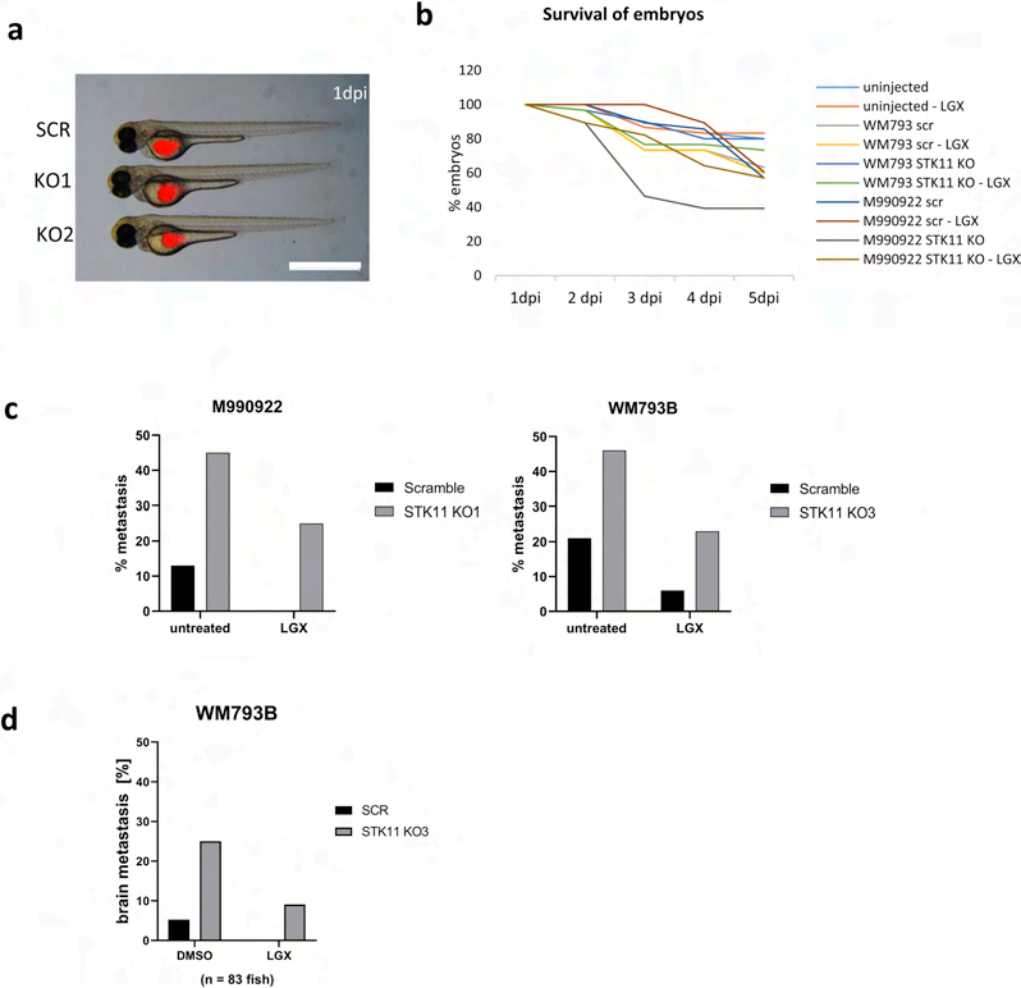
a
1dpi
SCR
KO1
KO2
b
Survival of embryos
% embryos
120
100
80
60
40
20
0
1dpi
2 dpi
3 dpi
4 dpi
5dpi
uninjected
uninjected - LGX
WM793 scr
WM793 scr - LGX
WM793 STK11 KO
WM793 STK11 KO - LGX
M990922 scr
M990922 scr - LGX
M990922 STK11 KO
M990922 STK11 KO - LGX
c
M990922
% metastasis
50
40
30
20
10
0
untreated
LGX
Scramble
STK11 KO1
WM793B
% metastasis
50
40
30
20
10
0
untreated
LGX
Scramble
STK11 KO3
d
WM793B
brain metastasis [%]
50
40
30
20
10
0
DMSO
LGX
(n = 83 fish)
SCR
STK11 KO3

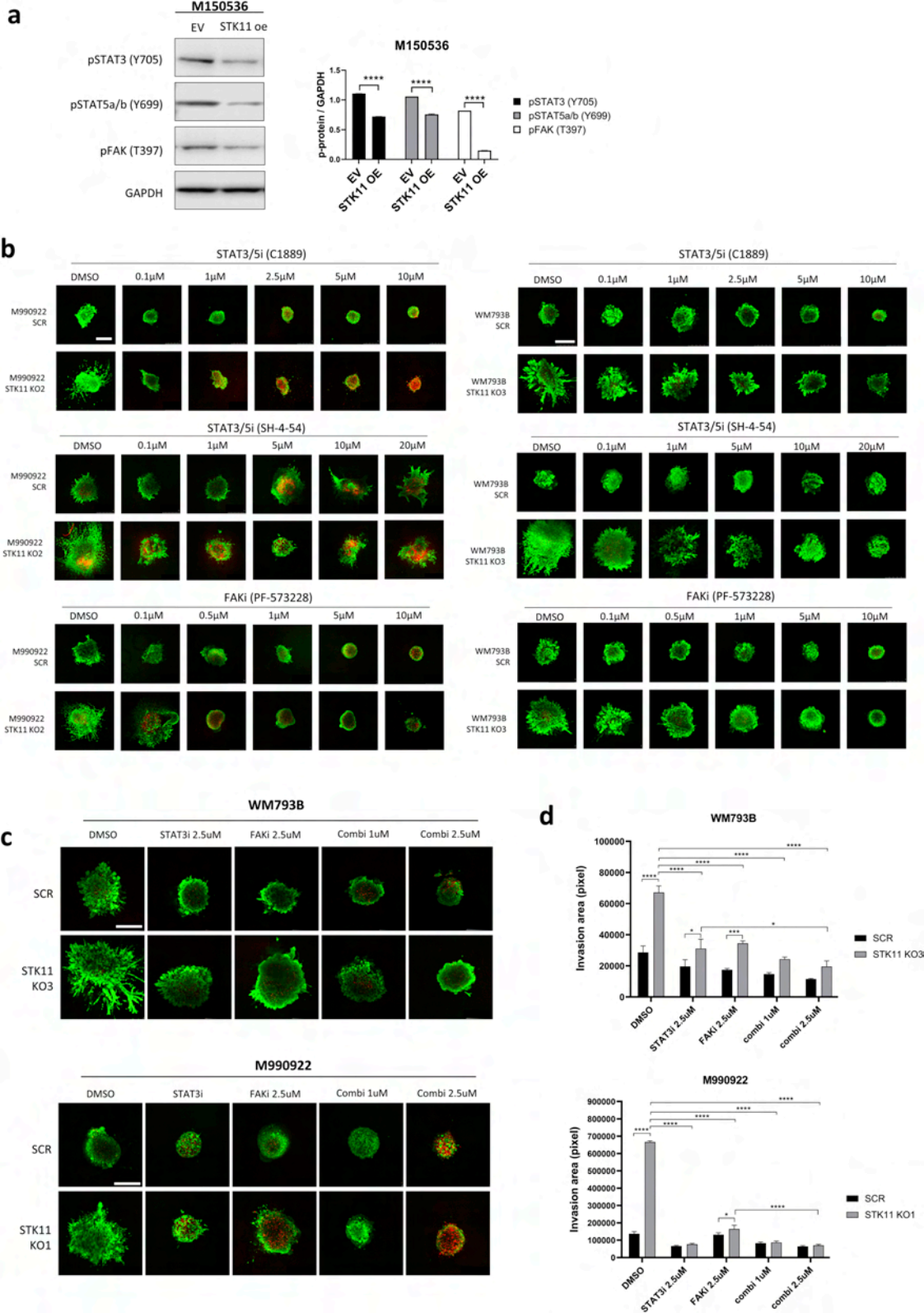
a
M150536
EV
STK11 oe
pSTAT3 (Y705)
pSTAT5a/b (Y699)
pFAK (T397)
GAPDH
M150536
p-protein / GAPDH
****
EV
STK11 OE
pSTAT3 (Y705)
pSTAT5a/b (Y699)
pFAK (T397)
b
STAT3/5i (C1889)
DMSO
0.1μM
1μM
2.5μM
5μM
10μM
M990922 SCR
M990922 STK11 KO2
WM793B SCR
WM793B STK11 KO3
STAT3/5i (SH-4-54)
20μM
FAKi (PF-573228)
0.5μM
c
WM793B
DMSO
STAT3i 2.5uM
FAKi 2.5uM
Combi 1uM
Combi 2.5uM
SCR
STK11 KO3
M990922
STAT3i
STK11 KO1
d
WM793B
Invasion area (pixel)
SCR
STK11 KO3
M990922
STK11 KO1

a

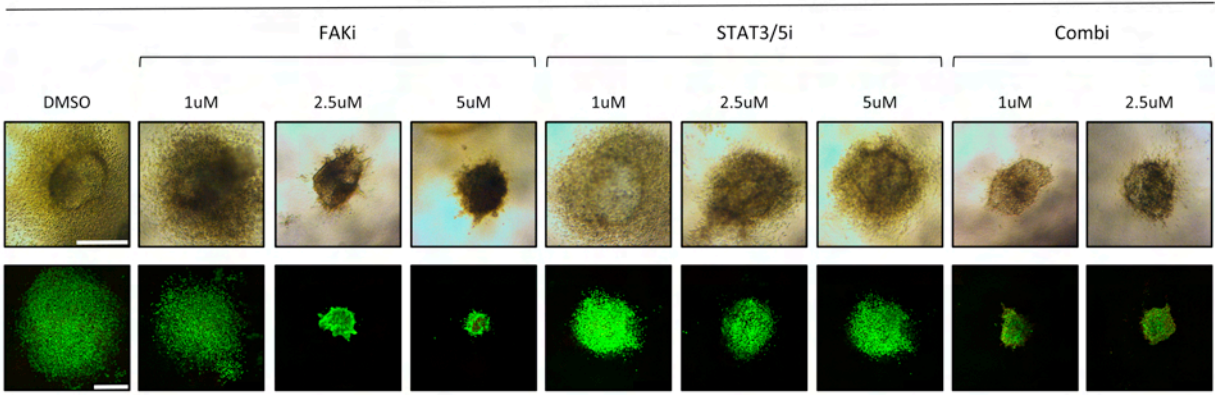
M130425 - STK11 KO2
FAKi
STAT3/5i
Combi
DMSO
1uM
2.5uM
5uM
1uM
2.5uM
5uM
1uM
2.5uM

b

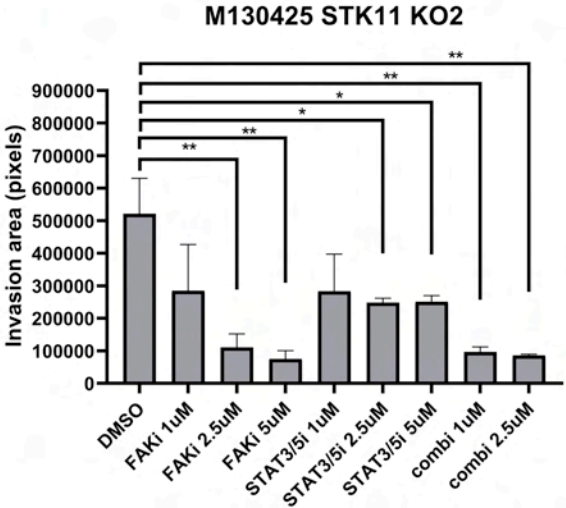
M130425 STK11 KO2
Invasion area (pixels)
900000
800000
700000
600000
500000
400000
300000
200000
100000
0
**
**
*
*
**
**
DMSO
FAKi 1uM
FAKi 2.5uM
FAKi 5uM
STAT3/5i 1uM
STAT3/5i 2.5uM
STAT3/5i 5uM
combi 1uM
combi 2.5uM